An 83,000 year old ice core from Roosevelt Island, Ross Sea, Antarctica

James E. Lee[1], Edward J. Brook[1], Nancy A. N. Bertler[2,3], Christo Buizert[1], Troy Baisden[3,4], Thomas Blunier[5], V. Gabriela Ciobanu[5], Howard Conway[6], Dorthe Dahl-Jensen[5], Tyler J. Fudge[6], Richard Hindmarsh[7], Elizabeth D. Keller[3], Frédéric Parrenin[8], Jeffrey P. Severinghaus[9], Paul Vallelonga[5], Edwin D. Waddington[6], and Mai Winstrup[5]

[1]College of Earth, Ocean, and Atmospheric Sciences, Oregon State University, Corvallis, OR 97331, USA
[2]Antarctic Research Centre, Victoria University of Wellington, Wellington, New Zealand
[3]GNS Science, Gracefield, Lower Hutt, 5010, New Zealand
[4]Now at Faculty of Science and Engineering, University of Waikato, Hamilton, New Zealand
[5]Centre for Ice and Climate, Niels Bohr Institute, University of Copenhagen, Copenhagen, Denmark
[6]Department of Earth and Space Sciences, University of Washington, Seattle, WA 98195, USA
[7]British Antarctic Survey, Cambridge CB3 0ET, United Kingdom
[8]University Grenoble Alpes, Centre National de la Recherche Scientifique, Institut de Recherche pour le Développement, Institut des Géosciences de l'Environnement, 38000 Grenoble, France
[9]Scripps Institution of Oceanography, University of California, San Diego, La Jolla, CA 92093, USA

Correspondence: James E. Lee (JLee@COAS.OregonState.edu)

Abstract. In 2013, an ice core was recovered from Roosevelt Island in the Ross Sea, Antarctica, as part of the Roosevelt Island Climate Evolution (RICE) project. Roosevelt Island is located between two submarine troughs carved by paleo-ice-streams. The RICE ice core provides new important information about the past configuration of the West Antarctic Ice Sheet and its retreat during the most recent deglaciation. In this work, we present the RICE17 chronology and discuss preliminary obser-

5   vations from the new records of methane, the isotopic composition of atmospheric molecular oxygen ($\delta^{18}O_{atm}$), the isotopic composition of atmospheric molecular nitrogen ($\delta^{15}N$-N_2), and total air content (TAC). RICE17 is a composite chronology combining annual layer interpretations, gas synchronization, and firn modeling strategies in different sections of the core. An automated matching algorithm is developed for synchronizing the high-resolution section of the RICE gas records (60-720 m, 1971 CE to 30 ka) to corresponding records from the WAIS Divide ice core, while deeper sections are manually matched. Ice

10   age for the top 343 m (2635 yr BP, before 1950 C.E.) is derived from annual layer interpretations and described in the accompanying paper by Winstrup et al. (2017). For deeper sections, the RICE17 ice age scale is based on the gas age constraints and the ice age-gas age offset estimated by a firn densification model.

Novel aspects of this work include: 1) stratigraphic matching of centennial-scale variations in methane for pre-anthropogenic time periods, a strategy which will be applicable for developing precise chronologies for future ice cores, 2) the observation

15   of centennial-scale variability in methane throughout the Holocene which suggests that similar variations during the late pre-industrial period need not be anthropogenic, and 3) the observation of continuous climate records dating back to ~65 ka which provide evidence that the Roosevelt Island Ice Dome was a constant feature throughout the last glacial period.

1 Introduction

The stability of the West Antarctic Ice Sheet (WAIS) is one of the largest uncertainties in predicting future sea level rise (Church et al., 2013; Jevrejeva et al., 2014; Golledge et al., 2014; Pollard et al., 2015; DeConto and Pollard, 2016). Much of the ice sheet is grounded below sea level with the bed deepening towards the center of the ice sheet. If the ice sheet were to retreat,

5 the grounding line would move to deeper water depths where it is physically less stable (a phenomenon known as marine ice sheet instability, Hughes 1973; Weertman 1974; Schoof 2007; Feldmann and Levermann 2015) and more vulnerable to undercutting by "warm" subsurface currents (Robin and Adie, 1964; Shepherd et al., 2004) and ice cliff instability (DeConto and Pollard, 2016) promoting enhanced ice flow and further mass loss. Vulnerability of WAIS to future warming can be assessed by investigating how it has responded to different climate regimes in the past. Unfortunately, geologic evidence of the

10 past size and extent of Antarctic ice sheets is spatially sparse, tends to have large chronological uncertainty, and is sometimes contradictory (Whitehouse et al., 2012; Anderson et al., 2014; Bentley et al., 2014; Clark and Tarasov, 2014; Halberstadt et al., 2016; McKay et al., 2016).

The Ross Embayment is the largest drainage of WAIS, both in terms of area and mass loss (Halberstadt et al., 2016). The glacial history of WAIS in the Ross Sea has been speculated about since Captain James Ross first mapped its edge in 1841-1842,

15 followed by the first geologic studies of the region during the Discovery, Nimrod, and Terra Nova expeditions (Scott, 1907; David et al., 1910-11; Debenham, 1921). In the modern era, two basic scenarios have been proposed for the configuration of WAIS in the Ross Embayment during the Last Glacial Maximum (LGM) (Stuiver et al., 1981). First, in the "maximum scenario," a thick and grounded ice sheet in the Ross Sea extended to the continental shelf break (Denton et al., 1989). Details of this scenario are supported by geomorphic features including grounding-zone wedges, which form at the terminus of marine

20 based glaciers (Shipp et al., 1999), and over-compressed diamictons, which are the result of thick overlying ice (Anderson et al., 1984, 1992). Evidence of high stands in the Transantarctic Mountains and the islands of the western Ross Sea (Denton and Marchant, 2000) as well as cosmogenic exposure dates on nunataqs in Marie Byrd Land (Stone et al., 2003) also support this idea. In an alternate scenario, Denton et al. (1989) proposed that grounded ice in the Ross Sea was kept thin by fast-flowing ice streams. In this scenario, the retreat of WAIS during the last deglaciation may not have contributed significantly to sea level

25 change. Studies of ice cores from Byrd Station (Steig et al., 2001) and Siple Dome (Waddington et al., 2005), glacial modeling (Parizek and Alley, 2004), and cosmogenic exposure dates from the Ohio Range (Ackert et al., 1999, 2007) all support this "minimal scenario."

In 2013, an ice core was drilled at the divide of Roosevelt Island as part of the Roosevelt Island Climate Evolution (RICE) project. Roosevelt Island is an ice dome located on a submarine plateau (∼200 mbsl) dividing the Whales Deep and Little

30 America Basins in the eastern Ross Sea (Fig. 1). During the LGM, these troughs were presumably occupied by the extension of the modern Bindschadler and MacAyeal ice streams (Ice Streams D and E, respectively) (Shipp et al., 1999), and Roosevelt Island would have been located along the main ice flow of WAIS. One motivation for the RICE project was to acquire a well-dated ice core that could be used in combination with geophysical measurements to unravel the glacial history of the eastern Ross Sea (Conway et al., 1999; Bertler, 2018, *personal communication*).

In this paper we first present measurements of methane, the isotopic composition of molecular oxygen ($\delta^{18}O_{atm}$), the isotopic composition of molecular nitrogen (δ^{15}N-N$_2$), and total air content (TAC). We use these datasets to establish the RICE17 chronology for the deeper section of the RICE ice core, a composite chronology combining annual layer interpretations (Winstrup et al., 2017), gas synchronization, and modeling of the ice age-gas age offset. The gas age-scale was synchronized by

5 (1) an automated matching routine, adapted from Huybers and Wunsch (2004) and novel in the application to ice cores, which simultaneously matched methane and $\delta^{18}O_{atm}$ records from RICE to records from the WAIS Divide ice core on the WD2014 age-scale (0-720 m, present-30 ka), (2) by visual matching to records from WAIS Divide for the lower-resolution section (720-746 m, 30-64.6 ka), and (3) by visual matching to records from the NGRIP ice core on a modified GICC05modelext chronology for ages older than WD2014 (746-752.95 m, 64.6-83 ka). Ice below 753 m is highly thinned, potentially disturbed

10 and the gas age could not be identified. The RICE17 ice age-scale for the top 343.7 m (2649 yr BP, before 1950 C.E.) is based on annual layer interpretations (Winstrup et al., 2017). Below this depth, ice age was derived from the gas age-scale by adding the ice age-gas age offset, estimated with a dynamic firn densification model (firn is the the upper layer of an ice sheet where snow compacts and transforms into ice, Buizert et al. 2015).

The approach used to develop the RICE17 age-scale is not unique for deep ice cores (Buizert et al., 2015), but includes

15 several refinements of the chronological techniques in order to improve the dating accuracy. Primarily, the RICE17 chronology benefited from the availability of high-resolution gas records from the WAIS Divide ice core. Centennial-scale variability of methane was well-captured in both the RICE and WAIS Divide ice core for the last 30 ka, a mode of variability previously limited for synchronization to the late Preindustrial Holocene due to the resolution of available records (Mitchell et al., 2011, 2015). The simultaneous matching of high-resolution records of methane and $\delta^{18}O_{atm}$ increased the strength of gas age

20 constraints. Finally, synchronization by an automated matching algorithm allowed for refinement of the age-scale with a Monte Carlo approach.

RICE17 is a continuous chronology, absent of discontinuities and with monotonically increasing age with depth, until at least 64.6 ka. The oldest age near the bottom of the core has a minimum of 83 ka. All ages are reported as years before present (BP), where present is defined as 1950 C.E.

25 **2 The Roosevelt Island ice core**

The 763 m long RICE ice core was drilled to bedrock near the summit of Roosevelt Island, in the eastern Ross Sea in West Antarctica (79.36° S, 161.71° W; elev. 550 m above sea level, Fig. 1). In addition to the main deep core, a shallow core was drilled to 20 m and several snow pits were sampled to understand recent climate (Bertler et al., 2018). Local mean annual air temperature is -23.5° C and annual snow accumulation is estimated to be ∼0.22 m ice equivalent, based on annual layers in

30 snow pits (Bertler et al., 2018). A cooler estimate of modern temperature, -27.4 ± 2.4° C based on ERA interim data from 1979-2012, was presented in Bertler et al. (2018), but this estimate is cooler than borehole thermometry measurements and previously published estimates (Herron and Langway, 1980; Conway et al., 1999; Martín et al., 2006) and does not provide a good fit to the density profile in the firn model. Other estimates of recent accumulation at the RICE drill site range from 0.18

m ice per year to 0.27 m ice per year, depending on method and time period (Winstrup et al., 2017; Bertler et al., 2018; Herron and Langway, 1980; Conway et al., 1999; Kingslake et al., 2014).

3 New data sets from the RICE ice core

3.1 Methane measurements

5 The RICE discrete methane record was measured at Oregon State University (OSU) following methods described by Mitchell et al. (2011, 2013) with updates described in Appendix A. A total of 702 samples were measured at 583 distinct depths between 60-753 m (Fig. 2a, e). Samples from 406 depths were measured between 60 and 670 m, dating from ~1970 C.E. to 11.87 ka, with a mean sample spacing of 28.75 years. Between 670 and 718.13 m the record spans 11.87 to 29.9 ka; 96 samples in this interval provide age resolution of 189 years. Age resolution decreases significantly for deeper depths. The interval from 718.53

10 to 746.00 m corresponds to 30.1-64.6 ka and the methane record has a mean resolution of 548 years. The deepest dated ice is at 752.95 m and has an age of 83 ka ($\pm$2 ka).

Methane was also measured continuously with a laser spectroscopy technique (Stowasser et al., 2012; Rhodes et al., 2013) during two separate continuous flow analysis (CFA) campaigns at GNS Science (Gracefield, New Zealand) in 2013 and 2014 (Pyne et al., 2018). The CFA methane record was affected by variability of air flow to the measurement instrument and fractures

15 within the core which allowed drill fluid and modern air into the melt head. Exclusion of these artifacts caused significant gaps in the record, particularly at depths below 676 m (12.6 ka). We consider the CFA methane record to be a supplement to the more robust but lower resolution discrete data set. Between 29.9-59.1 ka, the CFA methane record is critical for establishing age control. Below ~746 m (64.6 ka), the CFA methane record is difficult to interpret because of gaps in the record, uncertainty in measurement depth, and uncertainty in the calibration of CH_4 (Appendix B).

20 Several anomalously high discrete methane measurements appear between 44.6-50.9 ka (729.05-736.05 m) and below 64.6 ka (746 m) (Fig. 3a). In the former interval, methane is enriched by ~30 ppb compared with the WAIS Divide CFA methane record (Rhodes et al., 2015). Many samples in this section included fractures which can enclose modern air in the ice sample if they heal (Aydin et al., 2010). All RICE ice core samples deeper than 500 m were visually inspected for fractures as they were prepared for measurement and for drill fluid during extraction. In fractured ice it was common to see drill fluid in the flask as

25 the samples were melted for gas extraction. However, neither observation was a strong indicator that a sample would have an elevated methane concentration. None of these high concentration results were rejected.

3.2 Total air content measurements

Total air content (TAC) is defined as the amount of air per gram of ice in units of cm^3 air at STP/g ice. TAC (Fig. 2d, h) was measured at OSU as part of the methane concentration measurement following methodology of Mitchell et al. (2015) and

30 updates from Edwards et al. (in prep). TAC is influenced by accumulation and temperature, seasonal gradients in the firn related

to insolation (Raynaud et al., 2007), thermal gradients in the firn from multi-annual climate trends, and surface air pressure (Martinerie et al., 1992; Raynaud and Whillans, 1982).

Air trapped in bubbles, clathrates, or fractures intersecting the surface of the sample is lost, an effect called the cut-bubble effect (Martinerie et al., 1990). The cut-bubble effect is difficult to quantify, especially in ice which contains fractures through

5 which air may be lost. No correction for the cut-bubble effect was applied to the TAC measurements presented here. Samples were cut to uniform shapes whenever possible to ensure that the cut-bubble effect was relatively constant in order to limit the influence it has on the variability of the TAC record. TAC analysis was rejected when the cut-bubble effect was believed to greatly impact the results, such as in samples which fractures could not be excluded or were excluded by cutting the sample into irregular shapes or into multiple pieces. Of the 706 samples measured at OSU for TAC, 165 results were rejected based upon

10 visual inspection of the sample. Many of these came from the 670-752.95 m (11.7-83 ka) interval where only 58 of 177 TAC measurements are considered reliable. Nonetheless, the TAC record from the RICE ice core appears remarkably consistent (Fig. 3d).

3.3 $\delta^{18}O_{atm}$ and $\delta^{15}N$-N_2 measurements

$\delta^{18}O_{atm}$ and $\delta^{15}N$-N_2 were measured on samples adjacent to the discrete methane samples (Fig. 2b, f and c, g, respectively).

15 Analysis was conducted at Scripps Institution of Oceanography following Petrenko et al. (2006) and Severinghaus et al. (2009). Pooled standard deviation of replicate measurements for $\delta^{18}O_{atm}$ is 0.006‰ and for $\delta^{15}N$-N_2 is 0.0027‰ (both scales are relative to modern atmospheric composition).

Variations of $\delta^{18}O_{atm}$ are primarily caused by changes in low-latitude rainfall that affect the $\delta^{18}O$ of leaf water used in photosynthesis (Severinghaus et al., 2009; Landais et al., 2007, 2010) and changes in seawater $\delta^{18}O$ caused by ice sheets on

20 glacial cycles (Horibe et al., 1985; Bender et al., 1985, 1994; Sowers et al., 1993). Importantly, these variations are well known in independently dated ice cores and the atmosphere is well mixed on the relevant timescales, so $\delta^{18}O_{atm}$ variability may be used as a chronostratigraphic marker (Bender et al., 1994). These variations are well sampled in the RICE record until ∼64.6 ka (746.00 m), beyond which the chronology is no longer continuous.

Molecular N_2 in the atmosphere is isotopically stable over very long time-scales (Hattori, 1983; Sowers et al., 1989). Vari-

25 ability of $\delta^{15}N$-N_2 in the ice core record primarily reflects changes in gravitational fractionation and thermal fractionation within the firn which primarily result from changes in surface temperature and accumulation rate (Schwander, 1989; Sowers et al., 1989).

4 Strategy for developing the chronology

Annual layer counting strategies have been used to construct some of the most precise chronologies for ice cores, for example

30 the Greenlandic ice cores composite chronology (GICC05) which extends to 60 ka (Svensson et al., 2008) and the Antarctic WAIS Divide WD2014 chronology which is dated with annual layer interpretations through the last 31 ka (Sigl et al., 2016). Annual layer counting for the RICE ice core provided a timescale to 343.7 m depth, extending to 2649 yr BP (Winstrup et al.,

2017), using Straticounter, a multi-proxy automated layer counting algorithm (Winstrup et al., 2012; Winstrup, 2016). For the RICE ice core, below the most recent 100 years annual layers were interpreted from variations in pH, dust, black carbon, Ca^{+2}, and conductivity with a further constraint from a single absolute age marker at 165.02 m depth corresponding to 1251 C.E. (Winstrup et al., 2017).

5   No absolute age markers were found prior to 1251 C.E. and annual layers are too thin to distinguish prior to 2649 yr BP. The best chronological constraints for this section are measurements of methane and $\delta^{18}O_{atm}$, which we use to synchronize RICE with corresponding records from other ice cores with established chronologies. The RICE records are synchronized in four different sections. (1) Between present and 11.7 ka (48-670 m) and (2) from 11.7-30.66 ka (670-719.3 m), an automated synchronization routine was used to value match methane and $\delta^{18}O_{atm}$ records from RICE and WAIS Divide ice cores (Section

10   4.1). Separating these two time periods allowed for a better match for the 0-11.7 ka section, where sample resolution was better and variations of atmospheric methane were smaller (Fig. 3). (3) For the interval between 30.66 and 64.6 ka (719.30-746.00 m), a set of age control points (ACPs) were visually chosen to match methane and $\delta^{18}O_{atm}$ records from the RICE ice core to records from the WAIS Divide ice core on the WD2014 chronology (Table 1). (4) The discontinuous section, below 746 m (64.6 ka), is beyond the age of the WAIS Divide ice core, and target records for methane and $\delta^{18}O_{atm}$ were developed from

15   records from the NGRIP ice core (Landais et al., 2007; Baumgartner et al., 2014) (Section 4.2). A modification was made to the GICC05modelext age-scale for NGRIP (Wolff et al., 2010; Kindler et al., 2014) for consistency with the WD2014 chronology (Section 4.2).

An ice age-scale for RICE was obtained by adding Δage to the gas ages. Δage is estimated using a dynamic firn densification model (Buizert et al., 2015) constrained by past lock-in depth (LID) determined from $\delta^{15}N$-N_2, temperature determined

20   from δD (Bertler, 2018, *personal communication*) and borehole temperature (Bertler et al., 2018; Clemens-Sewall et al., Unpublished). Description of the Δage model is provided in Section 4.4.

As discussed above, the final RICE17 ice age-scale merges the annual layer counts and the gas-derived ice age-scale developed here. Good agreement between the two ice age-scales obviates any need to adjust either chronology at the transition depth. This strategy respects the higher resolution and lower uncertainty of the annual layer interpretations of ice age. The

25   ACPs, additional control points from the synchronization routine (floating control points, discussed below), and gas and ice ages in RICE17 for evenly spaced depths are provided in the supplementary material.

4.1   An automated matching algorithm for synchronizing ice core records: 0-30 ka

For the purpose of synchronizing between gas records, an automated matching algorithm was adapted from Huybers and Wunsch (2004). The method starts with a set of prior ACPs which all correspond to well defined variations in either methane

30   or $\delta^{18}O_{atm}$ (Table 1). Age uncertainty of ACPs was estimated from the length of time between 25% and 75% of the observed change of relevant variable. The goal of the routine is to iteratively adjust the interpolation between ACPs to improve a goodness-of-fit parameter by following steps 1-9 described below.

"Goodness-of-fit" is calculated as the χ^2 value comparing the normalized methane record from the RICE ice core to expectant values interpolated from the WAIS Divide ice core plus the analagous χ^2 value comparing the normalized $\delta^{18}O_{atm}$

records. The algorithm can accept additional parameters for synchronization, such as CO_2 or N_2O, but methane and $\delta^{18}O_{atm}$ are currently the only two suitable parameters available for the RICE ice core. In this analysis, we have normalized both the methane and $\delta^{18}O_{atm}$ records to have the same mean (5) and variance (1) in order to equally weight their χ^2 values and their importance to the synchronization.

5   A realization starts by randomly perturbing the age of ACPs within their prescribed uncertainty (Table 1) to define an initial depth-age scale. The perturbed ACPs remain fixed throughout the realization. ACPs are given the subscript k, where k=1 is the youngest/shallowest ACP. The records are then broken into N subsections which are distributed between ACPs. Subsections are designated with a subscript i, where i=1,2,3,...N. Floating control points (FCPs) are defined as the bounding depths/ages of these subsections, which will include the initial ACPs. Prior to any perturbations, the durations of the subsections (Δt) are

10   approximately the same. We have chosen Δt to roughly match the recurrence interval of variations of methane in the reference record and so that each subsection contains about five methane and five $\delta^{18}O_{atm}$ samples. The following steps are repeated to optimize goodness-of-fit:

1. Random scaling factors (p_i), which perturb the durations of the subsections, are drawn for each subsection from a normal distribution of μ=1 and σ_1=0.25.

15
$$\Delta t'_i = \Delta t_i \cdot p_i$$

2. Because random perturbations will change the length of time between the initial ACPs, we apply a second scaling so the perturbed chronology remains consistent with the prior ACPs. In this case, ACP_k and ACP_{k+1} are the nearest gas ACPs bounding subsection i, respectively. ACP' is the perturbed age of the gas age constraint after step 1, and Δt^*_i is the duration of the subsection after the second scaling:

20
$$\Delta t^*_i = \Delta t'_i \cdot \left(\frac{ACP_{k+1} - ACP_k}{ACP'_{k+1} - ACP'_k} \right)$$

3. Mean "accumulation rate" of each subsection ($\overline{A}_i$) is calculated following Nye (1963), which assumes that the thickness of annual layers ($\overline{\lambda}_i$) is the product of their original thickness and their relative depth ($\frac{\overline{z}_i}{H}$):
$$\overline{A}_i = \overline{\lambda}_i \cdot \left(1 - \frac{\overline{z}_i}{H}\right)^{-1}$$

where $\overline{z}_i$ is the mid-depth of the subsection i, H is the thickness of the ice sheet, and both $\overline{z}_i$ and H are in ice equivalent

25   units.

Because the assumptions about thinning from Nye (1963) is too simple to describe the flow conditions at Roosevelt Island, we do not consider this result to be representative of the true accumulation history. The assumption is necessary for the purposes of interpolating age versus depth to ensure that annual layer thickness decreases smoothly between FCPs. An accumulation history that we believe is more accurate is calculated below with an alternative method, using a

30   dynamic firn model (Section 4.4).

4. A perturbed chronology is only accepted if:

(a) Intervals between FCPs (Δt_i^*) are within a factor of 10 of the initial durations,

$$\frac{1}{10} \cdot \frac{(t_{end} - t_1)}{N} < \Delta t_i^* < 10 \cdot \frac{(t_{end} - t_1)}{N}$$

(b) Mean "accumulation rates" are realistic ($\overline{A}_i > 0$ cm ice eq per yr, $\overline{A}_{max} < 75$ cm ice eq per yr), and

(c) Mean "accumulation rates" of adjacent subsections are within a factor of 2 of each other.

5   These conditions provide loose restrictions for continuity in the depth-age relationship although they may not be physically realistic for the site.

5. Ages for all RICE sample depths are interpolated from the perturbed FCPs (Step 3), assuming piece-wise constant accumulation between FCPs and a linearly decreasing thinning function (Nye, 1963).

6. Goodness-of-fit is calculated on the perturbed age-scale (goodness-of-fit = $\chi_{CH4} + \chi_{\delta 18Oatm}$).

10   7. When a perturbation improves the goodness-of-fit, that iteration becomes the base for subsequent perturbations.

8. The cycle is repeated until 20 sequential perturbations fail to improve the goodness-of-fit in step 6.

9. Starting with the FCPs from step 8, the above steps (1-8) are repeated 13 times, reducing the size of perturbations in step 1 from $\sigma_1 = \frac{1}{4}$ to $\sigma_{13} = \frac{1}{128}$.

A Monte Carlo analysis repeats these steps (Steps 1-9) 1000 times, initiated from a different prior depth-age relationship by
15   randomly perturbing ACPs within their age uncertainty (Table 1). We choose the best realization for gas age constraints for the RICE17 gas age-scale. Parameters used for the synchronization are given in Table 2 for both intervals; 60.05-670.13 m and 670.13-719.30 m. Code for the synchronization routine is provided as supplementary material.

Uncertainty in gas age constraints is calculated as the root-mean-square error of FCP ages from the 1000 Monte Carlo realizations (Fig 4d), although we acknowledge calculating uncertainty as a symmetric Gaussian error can overly simplify
20   the empirical distribution of possible ages for a given depth (Fig. 5). Assessing uncertainty in this way integrates two types of error. The first is the ability to exactly match timing of two features. This uncertainty is determined by how well features are resolved in the records, measurement error, and the limited degrees of freedom in synchronization (i.e. the synchronization routine assumes constant accumulation during each subsections in a piece-wise manner, although the true accumulation history is more likely to smoothly vary). The second type of error is analogous to deciding which feature in the reference record is the
25   correct match. For example, the methane peak centered at 459.05 m (4675 yr BP) is, in some realizations, instead matched to a different methane peak observed at ~4550 yr BP in the WAIS Divide record, providing two distinct age possibilities with some uncertainty about each (Fig. 5c).

4.2 Extending the chronology with visually matched gas age control points: 30-83 ka

Sample resolution of the RICE methane record below 719.3 m (30.66 ka) prevented use of the automated routine to synchronize
30   this section of core. Gas age control points were visually chosen between 719.30 m (30.66 ka) and 746.00 m (65.6 ka) and

between 746.00 and 752.95 m (∼83 ka) (Table 1). Between 719.30 (30.66 ka) and 746.00 m (65.6 ka), ACPs were visually chosen by comparing the RICE discrete and CFA methane records and the $\delta^{18}O_{atm}$ record to the WAIS Divide methane (Rhodes et al., 2015) and $\delta^{18}O_{atm}$ records (Buizert et al., 2015).

The WAIS Divide records and the WD2014 chronology end at 67.8 ka. For the deeper (older) section of the RICE ice

5 core, between 746.00-752.95 m, we build target records from records of methane and $\delta^{18}O_{atm}$ from the NGRIP ice core (Baumgartner et al., 2014; Landais et al., 2007, 2010). Using the NGRIP ice core is internally consistent with the WD2014 chronology, which is itself tied to a modified GICC05modelext age-scale between 30-67.8 ka (Buizert et al., 2015). For the methane target record, we account for the interpolar difference by linearly scaling the record from Baumgartner et al. (2014) using an empirical least-squares fit between the NGRIP and WAIS Divide methane records between 55-67.8 ka.

10 Buizert et al. (2015) found that the annual layer counted portion of the GICC05modelext chronology (0-60 ka) (Andersen et al., 2006; Svensson et al., 2008) is systematically younger than ages of corresponding features found in the U/Th absolute dated Hulu speleothem record. A fit to Hulu ages was optimized by scaling the GICC05modelext ages linearly by 1.0063. For the target records we adopt the same scaling as Buizert et al. (2015) for the annual layer counted section of NGRIP, ending at 60 ka in the GICC05modelext chronology and equating to 60.378 ka in WD2014 (and RICE17). Ages older than 60 ka

15 in the GICC05modelext chronology are derived from the ss09sea Dansgaard-Johnsen model (Johnsen et al., 2001; NGRIP Community Members, 2004) which is not susceptible to under counting of annual layers. This portion of GICC05modelext was stitched to the annual layer counts by subtracting a constant 705 years (Wolff et al., 2010). For this section of the target NGRIP records, a constant 378 years is added to the age from GICC05modelext starting at the depth corresponding to 60 ka in the GICC05modelext (60.378 ka in WD2014).

20 Synchronization between records requires the occurrence of identifiable features that are well sampled in both records. We estimate age uncertainty for this set of ACP's (ACP's older than 29.9 ka) as the larger of the sample spacing of the two records being synchronized, following methods of Brook et al. (2005). Gas age uncertainty is plotted in Fig. 4d. The largest uncertainty is ∼1500-1700 years and occurs between 41.7-47.6 ka, when the age-scale is very compressed and the RICE records are poorly sampled.

25 ## 4.3 Age control points in the disturbed ice: 746-753 m

Continuity of the RICE ice core appears to end at 746.00 m below surface, where a discontinuity of 20‰ is observed in the RICE δD record (746.00-746.10 m) (Fig. 6b) and a 0.35‰ change is observed between sequential $\delta^{18}O_{atm}$ samples (745.81 and 746.20 m) (Fig. 6c). Methane and $\delta^{18}O_{atm}$ values immediately above this discontinuity date this ice to the end of DO-18 (∼64.6 ka). This age is supported by very negative δD values and a trend to more enriched values at shallower depths

30 which is consistent with warming trends observed in other Antarctic ice cores at this time period (Buizert et al., 2015; EPICA Community Members, 2006; Petit et al., 1999; Parrenin et al., 2013) (Fig. 6f).

Figure 6 presents our best effort to date the ice in the disturbed section, between 746.00 and 752.95 m. Below, we discuss how the ages are assigned to different depth sections, starting with the shallowest portion. Dating folded ice remains challenging, and the solution we found may not be unique.

Immediately below the discontinuity, between 746.10-747.85 m, methane and $\delta^{18}O_{atm}$ values best match our target records during DO-20 between 74.5-77.3 ka (Fig. 6), although the RICE methane record appears ∼30 ppb too high. Dating of this section to DO-20 implies that either 9.4 ka of climate history is missing from the RICE ice core because climate was not recorded or that 9.4 ka is compressed into ∼10 cm of ice. Extremely thin layers can be explained by ice flow or by an absence

5 of accumulation, but the latter scenario would cause a collapse of the firn and $\delta^{15}N$-N_2 values approaching 0‰ which are not observed.

A cluster of samples between 747.85-750.46 m are ∼0.16‰ more enriched in $\delta^{18}O_{atm}$ than was observed in the shallower section dated to DO-20 (Fig. 6c). In the NGRIP, EDML, and Siple Dome ice cores, a long term trend in $\delta^{18}O_{atm}$ towards more enriched values is observed from 80 to 65 ka (Capron et al., 2010; Severinghaus et al., 2009; Landais et al., 2007) (Fig. 6g).

10 The enriched values between 748.34-750.46 m most likely indicate that this ice is younger than the adjacent shallower depths and the stratigraphic order is reversed. In this depth range, methane and $\delta^{18}O_{atm}$ values best match the atmospheric history of DO-19 between 71.8-74.3 ka (Fig. 6). Below 750.46 m, methane and $\delta^{18}O_{atm}$ return to values that best match DO-20.

The depth representing the top of the reversal (the shallowest depth where age begins to get younger at deeper depths) at 747.85 m is marked by a clear minimum in δD (Fig. 6b). The RICE CFA methane data also show a minimum in concentration

15 at this depth, but this record is very erratic during this interval and the coincidence of these two features may not be meaningful. The bottom of the reversal, with the youngest age observed in this section, coincides with another clear minimum in the RICE δD at 749.60 m (Fig. 6b) consistent with a cooling trend which is observed during DO-19 in other Antarctic records (EPICA Community Members, 2006).

We note that two significant measurement gaps exist in the RICE δD record, at 746.89-747.07 m and at 750.00-750.25 m

20 (red bars in Fig. 6b). A 12‰ shift in δD accompanies both of these gaps. The second measurement gap (750.46-750.56 m) is at nearly the same depth which separates the samples dating to DO-19 from the grouping immediately below dated to DO-20. The discontinuity of the δD record at these gaps may signify another hiatus in the climate record or highly contorted layers that are typically found around folds (Cunningham and Waddington, 1990; Alley et al., 1997; Thorsteinsson and Waddington, 2002; Waddington et al., 2001).

25 Below 750.46 meters, trends in methane and $\delta^{18}O_{atm}$ indicate that the age of ice continues to increase with depth until at least 753 m (∼83 ka). Age of this depth is constrained by a measured $\delta^{18}O_{atm}$ value of -0.175‰. Such a depleted value is rare and only occurs during periods of high sea-level and small ice sheets, the most recent time period prior to the Holocene being MIS-5a (80-85 ka) (Severinghaus et al., 2009; Capron et al., 2010; Petit et al., 1999; Landais et al., 2007). Negative values were observed at two other depths below 753 m (Fig. 2f), but the stratigraphic order of these depths is difficult to assess.

30 ## 4.4 Dynamic firn model to establish ice age

Movement of air within the firn causes gases trapped in ice cores to be younger than the ice encapsulating it; this gas age-ice age difference is commonly denoted Δage. Firn densification models are typically used to simulate past Δage (Schwander et al., 1997; Goujon et al., 2003). The largest source of error in reconstructing Δage is the input parameters, which are rarely well known. Using $\delta^{15}N$-N_2 as a proxy for past firn column thickness, and assuming δD (Bertler, 2018, *personal communication*)

records past site temperature faithfully, firn densification models can be run in an inverse mode to estimate both past Δage and accumulation rates (Buizert et al., 2014, 2015).

For the RICE ice core chronology, we use a dynamic version of the Herron-Langway model (Herron and Langway, 1980) which was also used for construction of the WD2014 chronology (Buizert et al., 2015). The model simulates firn compaction

5   rates as well as vertical heat diffusion and advection. The model domain is the full 763 m ice column at 0.5 m resolution; a time step of 1 year is used. The model simulates both gravitational enrichment of δ^{15}N-N$_2$ and fractionation in the presence of thermal gradients. The model is forced with a temperature history derived from a record of δD (Bertler, 2018, *personal communication*) assuming a constant isotope sensitivity of 6‰·K^{-1} (Brook et al., 2005) which, in conjunction with an assumed geothermal heat flux of 78 mW·m^{-2}, provides a good fit to the measured borehole temperature profile (Clemens-Sewall et al.,

10 Unpublished). This sensitivity for RICE is similar to that observed for West Antarctica (Stenni et al., 2017; Cuffey et al., 2016; Masson-Delmotte et al., 2008) but is somewhat higher than the sensitivity obtained by comparing the RICE isotope record to ERA interim data (Bertler et al., 2018). However, lower sensitivities decreased the fit of the modeled borehole temperature profile. The dependency of our Δage results to the assumed isotope sensitivity was explored in a model sensitivity test (Appendix C), and are incorporated into the Δage uncertainty estimates. The model further assumes a constant ice thickness, a constant 2

15 m convective zone similar to other high accumulation dome sites with low mean wind speeds (Kawamura et al., 2006; Landais et al., 2006), and surface firn density of 400 kg·m^{-3} to match the modern surface firn density.

In a first iteration, we assume a prior ice age-scale for the temperature history by adding a constant 150 years to the gas chronology (Section 4.1 and 4.2). A new Δage solution is then calculated using the dynamic firn densification model. The Δage solution (and thereby the ice age-scale) is refined iteratively until it no longer changes appreciably (consistent within ∼1

20 year).

The climate at Roosevelt Island, with high accumulation and relatively warm temperatures, is conducive to small Δage values, and consequently, relatively low absolute uncertainty in Δage compared to most Antarctic sites. Modern Δage (estimated at 60 m depth, the shallowest measurement of δ^{15}N-N$_2$) is 146 years with a reconstructed lock-in depth (LID) of 48 m, consistent with the modern density profile (Bertler et al., 2018; Winstrup et al., 2017). The Holocene Δage variations are small,

25 with Δage values ranging between 140 to 182 years. During the last glacial period, simulated Δage values fluctuate between ∼150-350 years.

Uncertainties in past Δage include the uncertainty of the parameters which constrain the model as well as in the model itself. The uncertainty of the Herron-Langway model is conservatively estimated to be 20%, based on differences between firn models (Lundin et al., 2017). We assessed the uncertainty due to model inputs using a steady-state Herron-Langway model

30 that approximates the dynamic version but requires less computational time (Appendix C). In a sensitivity test, we randomly perturb the parameterizations of temperature and LID and assumptions of convective-zone thickness, surface firn density, and geothermal heat flux and recalculate the Δage solution (model parameters and their base values and ranges used in the sensitivity test are provided in Table A1). A total of 6000 iterations were run. Model sensitivity is the root-mean-square-error of Δage calculations for each depth. Combined Δage uncertainty, provided in the included age-scale, is the root-sum-squares

35 of the model uncertainty and the model sensitivity.

4.5 Comparison of gas-derived and layer counted chronologies: 0-2,649 yrs BP

The gas-derived ice age-scale provides a chronology from 60 to 753 m depth (Fig. 2) that is independent of and overlaps the annual layer counted section (0-343.7 m, Winstrup et al. 2017). Figure 7a shows chronologies derived from annual layer counting and the gas-measurements. Differences between the two chronologies is shown in Fig. 7b (Positive values indicate

5 that the annual layer counts are older than the gas-derived ages). The gas-derived ice age-scale agrees well with the annual layer counted age-scale, within 33 years, with similar trends in the implied annual layer thickness (Fig. 7c). Differences between chronologies can result from the synchronization of gas records, calculation of Δage for either the RICE or WAIS Divide ice cores, interpolation between ACPs, or in counting of annual layers in the RICE ice core or the WAIS Divide ice core (used as a reference for the gas age-scale).

10 The average age difference at depths of FCPs is -1 years (n=18, implied age from gas-derived ice age-scale being older than the layer counted chronology). Root-mean-square of the age difference is 17.3 years. The gas-derived ice age-scale can also be compared to the age of 67 volcanic peaks identified in the RICE ice core and correlated to peaks identified in the WAIS Divide ice core (open red circles in Fig. 7, Winstrup et al. 2017). Compared to these volcanic peaks, the root-mean-square ice age difference of the gas-derived ice age-scale is 13.6 years from their WD2014 ages. Good agreement between the

15 two approaches gives confidence in the methodology used for the deeper section of the RICE17 chronology. The two largest differences occur at 89.72 m (243 yr BP) and at 169.11 m (757 yr BP) and are +30 years and -33 years, respectively (Fig. 7b). These offsets are similar in magnitude to the individual uncertainties in calculating Δage or in synchronizing the gas records. The small age differences between the two ice chronologies also indicates that our approach to calculating uncertainty is likely conservative.

20 The RICE17 transitions between the annual layer counted and gas-derived age-scales at 343.7 m, the deepest/oldest FCP for which annual layers were identifiable (Section 4.1). The age difference at this depth is 3 years, with the gas-derived ice age implying an older age than the annual layer counted chronology. This age difference is much less than the respective age uncertainties of 45 years and 111 years (2-σ) for the annual layer counts and gas-derived ice age-scale, respectively. Because of the good agreement between the two ice age-scales, no correction is made for the 3 year offset and the annual layer counted

25 age is used.

5 Results/key observations from the RICE chronology and gas data sets

5.1 New observations of centennial-scale variability in the Holocene methane cycle

Centennial-scale variability of methane in the late pre-industrial Holocene and Preboreal Holocene has been described from other records (Etheridge et al., 1998; Mischler et al., 2009; Sapart et al., 2012; Mitchell et al., 2013; Rhodes et al., 2017). The

30 methane records from the WAIS Divide and RICE ice cores are the highest resolution discrete records of the Holocene and the RICE CFA record is the first continuously measured record of the entire Holocene. Replication of centennial-scale variations in multiple ice cores demonstrates that they are robust features in the atmospheric history. These variations, which are well-

Climate
of the Past
Discussions
Open Access
EGU

defined in the RICE and WAIS Divide records, extend back to the last glacial period, providing new chronostratigraphic targets which can be used to date future ice cores, as we have done for matching the RICE and WAIS Divide ice cores.

Curiously, over the past 2,000 years, centennial-scale variability of methane only weakly correlates with temperature and precipitation of key methane producing regions (Mitchell et al., 2011), the main climatic factors controlling biogenic methane

5   production (Fung et al., 1991). The apparent lack of coherence with climatic forcing and changes in the stable isotopic composition of methane during this time period has led several studies to propose that this mode of variability may be linked to human population and early-anthropogenic land-use practices (Ferretti et al., 2005; Houweling et al., 2008; Mischler et al., 2009; Mitchell et al., 2011, 2013; Sapart et al., 2012). Anthropogenic forcing is supported by the coincidence of decreasing methane concentration with several well documented declines in global population resulting from disease or war (Mitchell

10   et al., 2011). All of these studies focused on ice core records of methane and the isotopes of methane during the past 2000 years when human population was significant enough to make this idea plausible. The RICE ice core documents that centennial-scale variability of similar magnitude and recurrence is prevalent throughout the last 11.7 ka (Fig. 3), before the rise of agriculture, when estimates of human populations were much lower. Recently, centennial-scale variability has also been documented in much older ice (Rhodes et al., 2017), dating from the last glacial period. This evidence implies that centennial-scale variability

15   can occur solely from natural forcing, but it is not currently clear what that forcing is.

5.2   Interpreting the accumulation history of Roosevelt Island from past firn structure

From 65 to 32 ka, low-variability of δ^{15}N-N$_2$ ranging from 0.20 to 0.24‰ suggests that changes in firn-thickness were also small (Sowers et al., 1989; Schwander, 1989) (Fig. 3c). The steady δ^{15}N-N$_2$ values in combination with the cooling trend observed in Antarctica for this time period suggest a decreasing trend in accumulation (Buizert et al., 2015).

20   While δ^{15}N-N$_2$ values appear steady from 65 to 32 ka and during the Holocene (Fig. 3c), they exhibit large variability between 32 and 10 ka (Fig. 8a). δ^{15}N-N$_2$ generally trends to heavier values beginning at 32 ka until 14.71 ka, indicating a growing firn column. An inflection point is observed at 25.3 ka which is interpreted as an acceleration of firn thickening concluding in a peak of 0.293‰ at 21.8 ka. After a short depletion the steep trend resumed with a second δ^{15}N-N$_2$ maximum of 0.326‰ reached at 15.7 ka. Following this maximum, δ^{15}N-N$_2$ abruptly decreased from 0.308‰ to 0.220‰ at 14.71 ka,

25   which corresponds with the beginning of the Antarctic Cold Reversal (ACR).

Between 25.3-32 ka, accumulation was ∼10 cm ice equivalent per year (Fig. 8d) and the increasing firn thickness is largely attributable to decreasing temperature. After 25.3 ka, accumulation starts to increase and by the first δ^{15}N-N$_2$ maximum (21.8 ka), accumulation had increased to ∼17 cm ice equivalent per year. By the second maximum (15.7 ka) accumulation increased to ∼25 cm ice equivalent per year, similar to accumulation rates observed during the Holocene. An accumulation

30   peak following glacial terminations is consistent with evidence from trimlines in interior WAIS (Ackert et al., 2013) and is also observed in the accumulation histories from WAIS Divide and Siple Dome (WAIS Divide Project Members, 2013; Waddington et al., 2005), but to a smaller degree. The early accumulation peak at 21.8 ka is unique to the RICE ice core.

A large, rapid depletion in the δ^{15}N-N$_2$ is observed at 14.71 ka with low values lasting until 12.38 ka. Curiously, this abrupt decrease in δ^{15}N-N$_2$ precedes the increase in CH$_4$ marking the onset of the Bølling-Allerød. In the firn model, this period of

shallow firn thickness is caused by a large reduction of snow accumulation (<10 cm/yr, Fig. 8d). Low accumulation during this period is consistent with thin annual layers interpreted from the age-depth relationship (Fig. 3d); 0.3-0.6 cm/yr annual layer thickness compared with 1.6-3.2 cm/yr between 10.09-11.01 ka (642.75-661.07 m). Following the ACR, at 12.38 ka, a rapid increase in accumulation is inferred, fully recovering to the ∼25 cm per year observed before the ACR.

A large accumulation gradient is observed across the Roosevelt Island ice dome (Winstrup et al., 2017) which implies that a period of low accumulation may be the result of regional climate changes or changes to the geometry of the Roosevelt Island ice dome. However, the long timescales required for ice dome migration may be to slow compared to the abrupt timescale of the inferred accumulation event. One mechanism which may cause rapid adjustment of the ice dome location is if the ice streams which surrounded and buttressed Roosevelt Island ice dome were suddenly removed (Ackert et al., 1999, 2013; Halberstadt et al., 2016). In this scenario, the removal of grounded ice around Roosevelt Island would likely have enhanced ice flow within the dome resulting in its thinning and thin annual layers. The timing of the low accumulation interval is similar to when dust records from an ice core from Taylor Dome (Aarons et al., 2016), a site located in the Transantarctic Mountains near the Ross Sea (Fig. 1), imply that the spatial extent of the Ross Ice Shelf withdrew and is similar to some estimates of the timing of retreat of the WAIS based on sediment facies succession and radiocarbon dating (minimum date of 8.6 ka, McKay et al. 2016) and also ice-sheet modeling (by meltwater pulse-1a, ∼14.7 ka, Golledge et al. 2014; McKay et al. 2016). Although annual layer thickness immediately above the ACR section is observed to be nearly five times as thick as the ACR section, this large change in thickness, if solely the result of changes in ice flow, would require an unrealistic change in the thickness of the dome or its ice flow which is not supported by TAC measurements or ice-flow modeling.

Based on physical arguments, our preferred explanation is that an interval of arid conditions between 12.38 and 14.71 ka resulted in a shallow firn structure and depleted δ^{15}N-N$_2$ values. In recent times, moisture arriving at Roosevelt Island is frequently related to enhanced cyclonic air flow in the Ross Sea and a strong Amundsen Sea Low (Tuohy et al., 2015; Emanuelsson et al., 2018). This period of low accumulation may indicate a changed atmospheric structure in the South Pacific where southward air flow is blocked by a persistent low pressure zone north of the Ross Sea such as observed in more recent periods in the accumulation record from RICE (Bertler et al., 2018; Emanuelsson et al., 2015) and potentially related to the past ice shelf extent. Such a pronounced minimum in accumulation is not observed in the Siple Dome ice core, where annual layers are observed to thicken during the ACR (Brook et al., 2005; Waddington et al., 2005). If non-thermal effects influenced the RICE δD record, which is interpreted as temperature in our firn model, then the magnitude of accumulation change during this period may not be as large as reconstructed from the firn model. While not currently available, measurements of d$_{excess}$, dust particle size distributions, and dust geochemistry may be helpful in explaining the temperature and accumulation history of RICE.

5.3 Implications for climate and ice sheet history

Early reconstructions of the Ross Ice sheet during the LGM were based on glacial geological constraints from the western margin of the embayment. They showed thick ice in the Ross Embayment that overrode both Siple Dome and Roosevelt Island (Denton and Hughes, 2002). However, more recent observations and model experiments indicate that Siple Dome was not

overrun by the interior ice sheet during the LGM (Waddington et al., 2005; Price et al., 2007) and that although the Ross ice streams likely slowed down during the LGM, they remained active, maintaining a low elevation profile of the ice sheet in the Ross Sea (Parizek and Alley, 2004).

Our results further support this scenario, and adds a key new constraint on ice thickness and thinning in the Eastern Ross Sea. Specifically, our results suggest that ice deposited on Roosevelt Island originated as accumulation local to the drilling site which may not be true if WAIS was thick during the LGM and overrode Roosevelt Island. If remnants of WAIS were stranded on Roosevelt Island, it may be recognized by a hiatus in the gas and ice chronology, by values of δD or TAC characteristic of more continental or much higher elevations, or discontinuities in the δ^{15}N-N_2 record indicating a much different firn structure.

While the RICE ice core chronology does exhibit at least one discontinuity in age (at 64.6 ka) as well as an age reversal, this does not coincide with the timing of the retreat of WAIS in the Ross Sea (McKay et al., 2016). The largest discontinuity, at 746.00-746.10 m, is accompanied by a 9.4 ka hiatus. However, the observed change in δD at RICE during this discontinuity is comparable to the change observed in the EDML ice core during the same time period, 65-69 ka and 71-79 ka (Fig. 6f). A possible second discontinuity is observed at 747.00 m depth at a small gap in measurements of 2.7 cm. Ice immediately below 747.00 m is interpreted as being warmer, meaning that this is probably not derived from somewhere upstream in WAIS at a higher elevation (Fig. 6b). Additionally, no dramatic or sudden change in δ^{15}N-N_2 or TAC was observed in association with this depth (Fig. 6). During the ACR, shifts in δ^{15}N-N_2 and TAC were observed (Fig. 3), however no discontinuities in δD were observed (Bertler, 2018, *personal communication*). We conclude that it is highly unlikely that the accumulation site of the RICE ice core changed during the deglaciation. This evidence leads us to believe that the Roosevelt Island ice dome probably remained independent of an advanced WAIS during the LGM. A similar conclusion was reached about Siple Dome during the LGM (Waddington et al., 2005; Nereson et al., 1998; Price et al., 2007; Parizek and Alley, 2004).

Geomorphological features on the Ross Sea bed do provide evidence of an expansive ice sheet which extended past Roosevelt Island during the LGM (Shipp et al., 1999; Anderson et al., 1984, 1992, 2014; Halberstadt et al., 2016). The stability of the Roosevelt Island ice dome and of Siple Dome implies that at this time, WAIS flowed around these sites rather than over them. This observation implies that as WAIS grew spatially, its thickness in the Ross Sea was limited, conditions that indicate ice streams were active throughout the last glacial period. Alternatively, Price et al. (2007) proposed that the geomorphological features observed in the eastern Ross Sea may represent building of an ice dome in Marie Byrd Land. The RICE records can not distinguish between these scenarios.

6 Conclusions

We present the RICE17 gas and ice chronologies for the RICE ice core. These timescales date the gas and ice records from the RICE ice core for the last ∼83 ka. Between 0-30 ka, an automated synchronization routine is used to identify gas age control points that best match the RICE methane and $\delta^{18}O_{atm}$ records to the respective records from the WAIS Divide ice core (WAIS Divide Project Members, 2013; Buizert et al., 2015). This technique requires few prior constraints, accommodates simultaneous synchronization of multiple parameters, and allows assessment of age uncertainty. Unique in this approach is

the use of centennial-scale variability of methane for chronostratigraphic matching for ages older than the last ∼2,000 years. Synchronization between ice cores for the time period between 30 and 83 ka (719-753 m) was accomplished by manually choosing tie-points. Below 753 m the ice could not be dated with the currently available data. The RICE17 ice age-scale is based on annual layer counts between -62 and 2649 yr BP (0-343.7 m) and for depths below 343.7 m, a separate ice age-scale

5 was derived from the synchronized gas age-scale by adding Δage estimated from a firn model.

Key contributions from the development of the RICE17 age scale include evidence of active ice streams in the Eastern Ross Sea during the last glacial cycle as well observations about pre-anthropogenic variations of methane. The former is supported by the continuous age-scale and continuous records of climate from RICE which imply that the Roosevelt Island ice dome remained stable and independent of WAIS for at least the last 64.6 ka and likely for the last 83 ka. The continuous record

10 of methane from the RICE ice core is the first covering the Holocene. Centennial-scale variability of methane is observed throughout the Holocene and in earlier periods. During the last 2000 years, this mode of variability has been attributed to the influence of early human activity (Ferretti et al., 2005; Houweling et al., 2008; Mischler et al., 2009; Mitchell et al., 2011, 2013; Sapart et al., 2012), although the prevalence of these variations prior to significant human populations implies that there may be some other explanation.

15 The RICE ice core provides records of climate, with precise dating, for a scarcely sampled region of Antarctica. Future work will investigate regional climate of the Eastern Ross Sea in comparison to climate records from other sites to better understand spatial patterns around Antarctica, such as during the ACR when Roosevelt Island experienced an interval of particularly low accumulation, and to study the glacial retreat of WAIS in the Ross Sea.

Code and data availability. The following will be made available on public archives: RICE prior age control points, RICE final age control

20 points, RICE17 age-scale interpolated at higher resolution, RICE CH_4, $\delta^{18}O$-O_2, and $\delta^{15}N$-N_2 data, and code for the gas synchronization routine.

Appendix A: Methane Measurements

Description of the methodology used at Oregon State University for measuring methane concentration in ice cores was described in Grachev et al. (2009) and Mitchell et al. (2013). To paraphrase, 40-60 g ice samples are trimmed and placed in glass

25 flasks. The glass flasks are then attached to a high vacuum line and immersed in a chilled ethanol bath set to -63°C to keep the samples frozen. Since Mitchell et al. (2013), insulation has been added around the ethanol bath and above where the flasks are mounted. The added insulation decreased the temperature variability of the ethanol bath and of the sample flasks throughout the day allowing for better measurement of pressure and improved signal-to-noise for the chromatograph.

After laboratory air has been evacuated, the flasks are closed and the samples are melted in a hot water bath for 30 minutes

30 to liberate air from the sample. Samples are then refrozen by immersing the flasks back into the cold ethanol bath. Once the samples are completely refrozen and the sample flask temperature has stabilized (approximately 1 hour after refreezing begins),

measurement of the sample for methane concentration is performed by expanding sample air from the flask headspace into a gas chromatograph (GC). A set of calibration measurements are made on dry compressed air of known methane concentration (standard gas) by varying the pressure of each run. Calibration runs are made both before and after samples are measured. The calibration curve is a least-squares linear regression between pressure and peak area for both sets of calibration runs described

5   by a slope m_{cal} and intercept b_{cal}.

Methane concentration (C) was previously calculated by comparing the sample pressure (P_{meas}) and the peak area (PA_{meas}) from GC analysis to the predicted peak area of the standard gas of equal pressure.

$$C_{raw} = C_{standard} \cdot \frac{PA_{meas} - b_{cal}}{P_{meas} \cdot m_{cal}} \tag{A1}$$

Four measurements can be made on each ice sample. If the two sets of calibration runs are taken individually, interpretation of

10   sample concentrations typically differ by <3 ppb.

In this calculation, the sample pressure is used to quantify the number of moles of air in the sample assuming that the sample temperature remains constant and equal to standard air temperature during calibration runs. However, in a series of dry blank experiments it was determined that sample gas temperature is cooler than the standard gas temperature. We estimate the temperature difference to be 0.42% of the standard air temperature and thus the sample pressure needs to be corrected upwards

15   by that amount. We call this the GC-thermal effect. We now apply the correction to the previous concentration calculation.

$$C_{raw} = C_{standard} \cdot \frac{PA_{meas} - b_{cal}}{P_{meas} \cdot 1.0042 \cdot m_{cal}} \tag{A2}$$

Results from typical wet blank samples, in which we add standard air over bubble free ice made from Milli-Q ultra-pure water, had shown that these samples are typically 2-3 ppb enriched compared to the standard concentration using the old method for calculating concentration. This agrees with the predicted magnitude of enrichment from the GC-thermal effect of 2.1 ppb.

20   Several wet blank samples are measured each day and are interspersed between ice core samples. The offset between the measured concentration of the wet blank and the known concentration of the standard gas added is called the "blank" correction. This represents any effects during the sample analysis process which may alter the measured concentration. We bin the wet blank results over the time period for which samples were measured to establish a single blank correction value with an estimated blank correction uncertainty. RICE ice core samples were measured during two separate periods and have separate

25   blank correction values.

Since the OSU analytical methods use a wet extraction technique to liberate ice core air, effects of gas solubility must be accounted for. Methane is more soluble than the major components of air and is preferentially dissolved during the extraction step. This leads to a decrease in the measured concentration compared to the true ice core concentration. Mitchell et al. (2013) empirically derived a solubility correction (S) which we repeated several times for the RICE samples. S is defined as the total

30   amount of methane (gas + dissolved) divided by the amount in gas phase. A solubility value of 1.0288 was used for ice core samples and 1.0112 for bubble free ice.

The "blank" and "solubility" corrections are applied in the following way:

$$C_{corrected} = C_{raw} \cdot S_{sample} - (C_{blank} \cdot S_{blank} - C_{standard}) \tag{A3}$$

This formula differs from that used by Mitchell et al. (2013). In Mitchell et al. (2013) no solubility correction was applied to the bubble free ice samples. The difference results in a constant offset of -7.4 ppb compared to Mitchell et al. (2013).

Appendix B: Calibration of RICE CFA methane

The RICE CFA methane record is qualitatively used for synchronization to the WAIS Divide methane record, and thus careful calibration was not required. Regardless, we present an ad hoc calibration of the RICE CFA methane record based on comparison to the RICE discrete methane record measured at Oregon State University (OSU). The RICE CFA methane record was measured in multiple campaigns and major adjustments and fixes to the analytical system occurred during both of those periods. Calibration of the RICE CFA record is done in a piecewise manner to reflect these changes.

Our calibration scheme accounts for instrument calibration, a concentration-based correction due to instrument sensitivity, and measurement drift, a time-dependent correction. For comparison between datasets, we subsample the CFA data at depths where discrete measurements were made. We first apply the concentration calibration by regressing the sub-sampled CFA methane concentration against the discrete measurement. Drift was accounted for by a second regression comparing the residual of the concentration calibration against either the measurement time or sample depth, which ever provided the better correlation to the discrete dataset. Drift was only a significant factor between 500-680 m depth. Calibration values are given in Table A2.

Uncertainty in the relationship may be caused by measurement uncertainty, which is relatively small, or the uncertainty in the depth registration of the continuous measurements. Uncertainty in the depth registration is relatively unimportant in the top ∼670 m of core. In this section, annual layers are relatively thick and the variability in methane is relatively low which results in only minor changes in methane concentration from an error in depth. However, for the deeper section of core, methane concentrations vary rapidly with depth and small errors in the depth registry represents large differences in methane concentration. Because of errors in the depth registry and the sensitivity of the inferred methane concentration, we restrict our calibration scheme to the last ∼39.66 ka (725.63 m) ending after the inclusion of GIS-8.

Appendix C: Steady-State Herron-Langway Sensitivity Test

The gas age-ice age offset (Δage) for the RICE ice core was estimated with a dynamic Herron-Langway model (Buizert et al., 2015). The model is constrained by measurements of δ^{15}N-N_2 (a proxy for firn thickness) and δD (a proxy for past temperature). The dynamic model also assumes a convective zone of 2 m, surface firn density of 400 kg·m^{-3}, and geothermal heat flux of 78 mW·m^{-2}.

A steady-state version of the Herron-Langway model mimics the dynamic version following a similar iterative methodology. A constant Δage estimate is assumed as a prior to assume an ice age scale for the temperature history. The model then calculates a new Δage solution from the temperature and firn thickness histories. This process is repeated until iterations no longer change appreciably.

While the dynamic version is used to establish the Δage history for RICE, the steady state version has the advantage of being computationally faster and is used in a sensitivity test. In this test, we vary prior assumptions about the isotopic temperature sensitivity used to infer past temperature, the convective zone thickness, surface firn density, and assumptions about geothermal induced temperature gradient in the firn. In a Monte Carlo approach, each parameter is given a range of acceptable values from which the steady-state Herron-Langway model calculates the Δage history (Table A1). This is repeated for 6000 realizations. Realizations are rejected if:

- The modeled modern ice age at lock-in depth (LID) is more than 25 years different than the annual layer counted age of that depth (48.57 m, 89 yrs BP).

- The modeled modern accumulation is less than 0.15 or greater than 0.35 m ice per year.

- The isotopic sensitivity is less than 3.2 or greater than 9.6 ‰·K^{-1}, similar to the range of values observed for West Antarctica (Masson-Delmotte et al., 2008; Cuffey et al., 2016; Stenni et al., 2017). This parameter is randomly chosen from a normal distribution at the beginning of each realization and can fall outside of this range.

- The minimum temperature is less than -60°C.

- The maximum estimated Δage is less than 1000 years.

- Modeled accumulation does not exceed 1.0 m ice per year and is never negative.

Δage is calculated for each depth that δ^{15}N-N$_2$ was measured. Uncertainty in Δage is assumed to be the root-mean-square-error of accepted realizations and is estimated for each sample depth.

References

Aarons, S., Aciego, S., Gabrielli, P., Delmonte, B., Koornneef, J., Wegner, A., and Blakowski, M.: The impact of glacier retreat from the Ross Sea on local climate: Characterization of mineral dust in the Taylor Dome ice core, East Antarctica, Earth and Planetary Science Letters, 444, 34–44, https://doi.org/10.1016/j.epsl.2016.03.035, 2016.

5   Ackert, R. P., Barclay, D. J., Borns, H. W., Calkin, P. E., Kurz, M. D., Fastook, J. L., and Steig, E. J.: Measurements of Past Ice Sheet Elevations in Interior West Antarctica, Science, 286, 276–280, https://doi.org/10.1126/science.286.5438.276, https://doi.org/10.1126/science.286.5438.276, 1999.

Ackert, R. P., Mukhopadhyay, S., Parizek, B. R., and Borns, H. W.: Ice elevation near the West Antarctic Ice Sheet divide during the last glaciation, Geophysical Research Letters, 34, https://doi.org/10.1029/2007GL031412, 2007.

10   Ackert, R. P., Putnam, A. E., Mukhopadhyay, S., Pollard, D., DeConto, R. M., Kurz, M. D., and Borns, H. W.: Controls on interior West Antarctic Ice Sheet Elevations: inferences from geologic constraints and ice sheet modeling, Quaternary Science Reviews, 65, 26–38, https://doi.org/10.7916/D8CG010P, 2013.

Alley, R. B., Shuman, C. A., Meese, D. A., Gow, A. J., Taylor, K. C., Cuffey, K. M., Fitzpatrick, J. J., Grootes, P. M., Zielinski, G. A., Ram, M., Spinelli, G., and Elder, B.: Visual-stratigraphic dating of the GISP2 ice core: Basis, reproducibility, and application, Journal of
15   Geophysical Research: Oceans, 102, 26 367–26 381, https://doi.org/10.1029/96jc03837, http://dx.doi.org/10.1029/96JC03837, 1997.

Andersen, K. K., Svensson, A., Johnsen, S. J., Rasmussen, S. O., Bigler, M., Röthlisberger, R., Ruth, U., Siggaard-Andersen, M.-L., Peder Steffensen, J., Dahl-Jensen, D., Vinther, B. M., and Clausen, H. B.: The Greenland Ice Core Chronology 2005, 15-42 ka. Part 1: constructing the time scale, Quaternary Science Reviews, 25, 3246–3257, https://doi.org/10.1016/j.quascirev.2006.08.002, 2006.

Anderson, J. B., Brake, C. F., and Myers, N. C.: Sedimentation on the Ross Sea continental shelf, Antarctica, Marine Geology, 57, 295–333,
20   https://doi.org/10.1016/0025-3227(84)90203-2, 1984.

Anderson, J. B., Shipp, S. S., Bartek, L. R., and Reid, D. E.: Evidence for a grounded ice sheet on the Ross Sea continental shelf during the late Pleistocene and preliminary paleodrainage reconstruction, Contributions to Antarctic Research III, pp. 39–62, https://doi.org/10.1029/AR057p0039, 1992.

Anderson, J. B., Conway, H., Bart, P. J., Witus, A. E., Greenwood, S. L., McKay, R. M., Hall, B. L., Ackert, R. P., Licht, K., Jakobsson,
25   M., et al.: Ross Sea paleo-ice sheet drainage and deglacial history during and since the LGM, Quaternary Science Reviews, 100, 31–54, https://doi.org/10.1016/j.quascirev.2013.08.020, 2014.

Aydin, M., Montzka, S. A., Battle, M. O., Williams, M. B., De Bruyn, W. J., Butler, J. H., Verhulst, K. R., Tatum, C., Gun, B. K., Plotkin, D. A., Hall, B. D., and Saltzman, E. S.: Post-coring entrapment of modern air in some shallow ice cores collected near the firn-ice transition: evidence from CFC-12 measurements in Antarctic firn air and ice cores, Atmospheric Chemistry and Physics, 10, 5135–5144,
30   https://doi.org/10.5194/acp-10-5135-2010, https://doi.org/10.5194/acp-10-5135-2010, 2010.

Baumgartner, M., Kindler, P., Eicher, O., Floch, G., Schilt, A., Schwander, J., Spahni, R., Capron, E., Chappellaz, J., Leuenberger, M., Fischer, H., and Stocker, T. F.: NGRIP CH_4 concentration from 120 to 10 kyr before present and its relation to a $\delta^{15}N$ temperature reconstruction from the same ice core, Climate of the Past, 10, 903–920, https://doi.org/10.5194/cp-10-903-2014, https://doi.org/10.5194/cp-10-903-2014, 2014.

35   Bender, M., Labeyrie, L., Raynaud, D., and Lorius, C.: Isotopic composition of atmospheric O_2 in ice linked with deglaciation and global primary productivity, Nature, 318, 349–353, https://doi.org/10.1038/318349a0, 1985.

Bender, M. L., Sowers, T., Barnola, J., and Chappellaz, J.: Changes in the O_2/N_2 ratio of the atmosphere during recent decades reflected in the
composition of air in the firn at Vostok Station, Antarctica, Geophysical Research Letters, 21, 189–192, https://doi.org/10.1029/93gl03548,
http://dx.doi.org/10.1029/93GL03548, 1994.

Bentley, M. J., Cofaigh, C. Ó., Anderson, J. B., Conway, H., Davies, B., Graham, A. G., Hillenbrand, C.-D., Hodgson, D. A., Jamieson, S. S.,

5   Larter, R. D., et al.: A community-based geological reconstruction of Antarctic Ice Sheet deglaciation since the Last Glacial Maximum,
Quaternary Science Reviews, 100, 1–9, https://doi.org/10.1016/j.quascirev.2014.06.025, 2014.

Bertler, N.: RICE δD-H_2O record, personal communication, data embargoed at time of submission., 2018, *personal communication*.

Bertler, N. A., Conway, H., Dahl-Jensen, D., Emanuelsson, D. B., Winstrup, M., Vallelonga, P. T., Lee, J. E., Brook, E. J., Severinghaus, J. P.,
Fudge, T. J., et al.: The Ross Sea Dipole-temperature, snow accumulation and sea ice variability in the Ross Sea region, Antarctica, over

10   the past 2700 years, Climate of the Past, 14, 193, https://doi.org/10.5194/cp-14-193-2018, 2018.

Brook, E. J., White, J. W. C., Schilla, A. S. M., Bender, M. L., Barnett, B., Severinghaus, J. P., Taylor, K. C., Alley, R. B., and Steig, E. J.:
Timing of millennial-scale climate change at Siple Dome, West Antarctica, during the last glacial period, Quaternary Science Reviews,
24, 1333–1343, https://doi.org/10.1016/j.quascirev.2005.02.002, https://doi.org/10.1016/j.quascirev.2005.02.002, 2005.

Buizert, C., Gkinis, V., Severinghaus, J. P., He, F., Lecavalier, B. S., Kindler, P., Leuenberger, M., Carlson, A. E., Vinther, B., Masson-

15   Delmotte, V., White, J. W. C., Liu, Z., Otto-Bliesner, B., and Brook, E. J.: Greenland temperature response to climate forcing during the
last deglaciation, Science, 345, 1177–1180, https://doi.org/10.1126/science.1254961, https://doi.org/10.1126/science.1254961, 2014.

Buizert, C., Cuffey, K. M., Severinghaus, J. P., Baggenstos, D., Fudge, T. J., Steig, E. J., Markle, B. R., Winstrup, M., Rhodes, R. H., Brook,
E. J., Sowers, T. A., Clow, G. D., Cheng, H., Edwards, L. R., Sigl, M., McConnell, J. R., and Taylor, K. C.: The WAIS Divide deep ice
core WD2014 chronology – part 1: Methane synchronization (68-31 ka BP) and the gas age-ice age difference, Climate of the Past, 11,

20   153–173, https://doi.org/10.5194/cp-11-153-2015, https://doi.org/10.5194/cp-11-153-2015, 2015.

Capron, E., Landais, A., Chappellaz, J., Schilt, A., Buiron, D., Dahl-Jensen, D., Johnsen, S. J., Jouzel, J., Lemieux-Dudon, B., Loulergue,
L., Leuenberger, M., Masson-Delmotte, V., Meyer, H., Oerter, H., and Stenni, B.: Millennial and sub-millennial scale climatic variations
recorded in polar ice cores over the last glacial period, Climate of the Past, 6, 345–365, https://doi.org/10.5194/cp-6-345-2010, https:
//doi.org/10.5194/cp-6-345-2010, 2010.

25 Church, J. A., Clark, P. U., Cazenave, A., Gregory, J. M., Jevrejeva, S., Levermann, A., Merrifield, M. A., Milne, G. A., Nerem, R. S., Nunn,
P. D., et al.: Sea-level rise by 2100, Science, 342, 1445–1445, https://doi.org/10.1126/science.342.6165.1445-a, 2013.

Clark, P. U. and Tarasov, L.: Closing the sea level budget at the Last Glacial Maximum, Proceedings of the National Academy of Sciences,
111, 15 861–15 862, https://doi.org/10.1073/pnas.1418970111, 2014.

Clemens-Sewall, D., Hawley, R., Conway, H., Brook, E., and Bertler, N.: Paleoclimate of the Ross Sea Region, from Roosevelt Island

30   Borehole Thermometry, Unpublished.

Conway, H., Hall, B., Denton, G., Gades, A., and Waddington, E.: Past and future grounding-line retreat of the West Antarctic Ice Sheet,
Science, 286, 280–283, https://doi.org/10.1126/science.286.5438.280, 1999.

Cuffey, K. M., Clow, G. D., Steig, E. J., Buizert, C., Fudge, T., Koutnik, M., Waddington, E. D., Alley, R. B., and Severinghaus, J. P.:
Deglacial temperature history of West Antarctica, Proceedings of the National Academy of Sciences, 113, 14 249–14 254, https://doi.org/

35   10.1073/pnas.1609132113, 2016.

Cunningham, J. and Waddington, E.: Boudinage: a source of stratigraphic disturbance in glacial ice in central Greenland, Journal of Glaciol-
ogy, 36, 269–272, 1990.

David, T. W. E., Priestley, R. E., and Shackleton, E. H.: British Antarctic Expedition, 1907-9, under the command of Sir E.H. Shackleton, c.v.o. Reports on the scientific investigations., vol. v. 1-2 Biology (1910-11), London,W. Heinemann,, http://www.biodiversitylibrary.org/item/62967, http://www.biodiversitylibrary.org/bibliography/22427 — Biology, edited by James Murray. — Geology, edited by T.W.E. David and R.E. Priestley. — The two volumes on biology were issued in parts, those of each volume paged continuously, and are without

5   title-pages. — "No further publications in this series are contemplated."–Publisher's announcement in Geology, v. 2, 1916. — [Ser. 1] Biology: vol. I. I. On collecting at Cape Royds, by J. Murray. 1910. II. On microscopic life in Cape Royds, by J. Murray. 1910. III. Antarctic Rotifera, by J. Murray. 1910. IV. Musci, by J. C, 1910-11.

Debenham, F.: British Antarctic ("Terra Nova") Expedition, 1910, Natural History Report: Recent and Local Deposits of McMurdo Sound Region, vol. Geology vol. 1, London,W. Heinemann, https://hdl.handle.net/2027/osu.32435013905740, 1921.

10   DeConto, R. M. and Pollard, D.: Contribution of Antarctica to past and future sea-level rise, Nature, 531, 591–597, https://doi.org/10.1038/nature17145, 2016.

Denton, G. H. and Hughes, T. J.: Reconstructing the Antarctic Ice Sheet at the Last Glacial Maximum, Quaternary Science Reviews, 21, 193–202, https://doi.org/10.1016/S0277-3791(01)00090-7, https://doi.org/10.1016/S0277-3791(01)00090-7, 2002.

Denton, G. H. and Marchant, D. R.: The geologic basis for a reconstruction of a grounded ice sheet in McMurdo Sound, Antarctica, at the last

15   glacial maximum, Geografiska Annaler: Series A, Physical Geography, 82, 167–211, https://doi.org/10.1111/j.0435-3676.2000.00121.x, 2000.

Denton, G. H., Bockheim, J. G., Wilson, S. C., and Stuiver, M.: Late Wisconsin and early Holocene glacial history, inner Ross embayment, Antarctica, Quaternary Research, 31, 151–182, https://doi.org/10.1016/0033-5894(89)90004-5, 1989.

Edwards, J., Brook, E., Buizert, C., Sowers, T., Alley, R. Severinghaus, J., Fegyveresi, J., Mitchell, L., Grechev, A., Ahn, J., Lee, J., and

20   Rebarchik, M.: High-resolution total air content from the GISP2 Ice Core: New insights into processes controlling pore volume during the firn ice transition, this manuscript contains descriptions of the methodology for the measurement and calculation of TAC as well as a compilation of datasets from samples previously measured at Oregon State University., in prep.

Emanuelsson, B., Baisden, W., Bertler, N., Keller, E., and Gkinis, V.: High-resolution continuous flow analysis setup for water isotopic measurement from ice cores using laser spectroscopy, Atmospheric Measurement Techniques, 8, 2869–2883, https://doi.org/10.5194/

25   amtd-7-12081-2014, 2015.

Emanuelsson, B. D., Bertler, N. A., Neff, P. D., Renwick, J. A., Markle, B. R., Baisden, W. T., and Keller, E. D.: The role of Amundsen–Bellingshausen Sea anticyclonic circulation in forcing marine air intrusions into West Antarctica, Climate Dynamics, pp. 1–18, https://doi.org/10.1007/s00382-018-4097-3, 2018.

EPICA Community Members: One-to-one coupling of glacial climate variability in Greenland and Antarctica, Nature, 444, 195–198,

30   https://doi.org/10.1038/nature05301, https://doi.org/10.1038/nature05301, 2006.

Etheridge, D. M., Steele, L. P., Francey, R. J., and Langenfelds, R. L.: Atmospheric methane between 1000 A.D. and present: Evidence of anthropogenic emissions and climatic variability, Journal of Geophysical Research, 103, 15 979–15 993, https://doi.org/10.1029/98jd00923, http://dx.doi.org/10.1029/98JD00923, 1998.

Feldmann, J. and Levermann, A.: Collapse of the West Antarctic Ice Sheet after local destabilization of the Amundsen Basin, Proceedings of

35   the National Academy of Sciences, 112, 14 191–14 196, https://doi.org/10.1073/pnas.1512482112, 2015.

Ferretti, D. F., Miller, J. B., White, J. W. C., Etheridge, D. M., Lassey, K. R., Lowe, D. C., Meure, C. M. M., Dreier, M. F., Trudinger, C. M., van Ommen, T. D., and Langenfelds, R. L.: Unexpected changes to the global methane budget over the past 2000 years, Science, 309, 1714–1717, https://doi.org/10.1126/science.1115193, https://doi.org/10.1126/science.1115193, 2005.

Fretwell, P., Pritchard, H. D., Vaughan, D. G., Bamber, J. L., Barrand, N. E., Bell, R., Bianchi, C., Bingham, R. G., Blankenship, D. D., Casassa, G., Catania, G., Callens, D., Conway, H., Cook, A. J., Corr, H. F. J., Damaske, D., Damm, V., Ferraccioli, F., Forsberg, R., Fujita, S., Gim, Y., Gogineni, P., Griggs, J. A., Hindmarsh, R. C. A., Holmlund, P., Holt, J. W., Jacobel, R. W., Jenkins, A., Jokat, W., Jordan, T., King, E. C., Kohler, J., Krabill, W., Riger-Kusk, M., Langley, K. A., Leitchenkov, G., Leuschen, C., Luyendyk, B. P., Matsuoka, K., Mouginot, J., Nitsche, F. O., Nogi, Y., Nost, O. A., Popov, S. V., Rignot, E., Rippin, D. M., Rivera, A., Roberts, J., Ross, N., Siegert, M. J., Smith, A. M., Steinhage, D., Studinger, M., Sun, B., Tinto, B. K., Welch, B. C., Wilson, D., Young, D. A., Xiangbin, C., and Zirizzotti, A.: Bedmap2: improved ice bed, surface and thickness datasets for Antarctica, The Cryosphere, 7, https://doi.org/10.5194/tc-7-375-2013, https://doi.org/10.5194/tc-7-375-2013, 2013.

Fung, I., John, J., Lerner, J., Matthews, E., Prather, M., Steele, L., and Fraser, P.: Three-dimensional model synthesis of the global methane cycle, Journal of Geophysical Research: Atmospheres, 96, 13 033–13 065, https://doi.org/10.1029/91JD01247, 1991.

Golledge, N., Menviel, L., Carter, L., Fogwill, C., England, M., Cortese, G., and Levy, R.: Antarctic contribution to meltwater pulse 1A from reduced Southern Ocean overturning, Nature Communications, 5, 5107, https://doi.org/10.1038/ncomms6107, 2014.

Goujon, C., Barnola, J. M., and Ritz, C.: Modeling the densification of polar firn including heat diffusion: Application to close-off characteristics and gas isotopic fractionation for Antarctica and Greenland sites, Journal of Geophysical Research: Atmospheres, 108, 18, https://doi.org/10.1029/2002jd003319, https://doi.org/10.1029/2002JD003319, 2003.

Grachev, A. M., Brook, E. J., Severinghaus, J. P., and Pisias, N. G.: Relative timing and variability of atmospheric methane and GISP2 oxygen isotopes between 68 and 86 ka, Global Biogeochemical Cycles, 23, https://doi.org/10.1029/2008GB003330, 2009.

Halberstadt, A. R. W., Simkins, L. M., Greenwood, S. L., and Anderson, J. B.: Past ice-sheet behaviour: retreat scenarios and changing controls in the Ross Sea, Antarctica, The Cryosphere, 10, 1003–1020, https://doi.org/10.5194/tc-10-1003-2016, https://doi.org/10.5194/tc-10-1003-2016, 2016.

Hattori, A.: Denitrification and dissimilatory nitrate reduction, pp. 191–232, Academic Press New York, 1983.

Herron, M. M. and Langway, C. C.: Firn densification: An empirical model, Journal Glaciology, 25, 373–385, https://doi.org/10.3189/S0022143000015239, 1980.

Horibe, Y., Shigehara, K., and Langway, C. C.: Chemical and isotopic composition of air inclusions in a Greenland ice core, Earth and Planetary Science Letters, 73, 207–210, https://doi.org/10.1016/0012-821X(85)90069-X, 1985.

Houweling, S., Van der Werf, G., Klein Goldewijk, K., Röckmann, T., and Aben, I.: Early anthropogenic CH_4 emissions and the variation of CH_4 and $^{13}CH_4$ over the last millennium, Global Biogeochemical Cycles, 22, https://doi.org/10.1029/2007GB002961, 2008.

Hughes, T.: Is the West Antarctic ice sheet disintegrating?, Journal of Geophysical Research, 78, 7884–7910, https://doi.org/10.1029/JC078i033p07884, 1973.

Huybers, P. and Wunsch, C.: A depth-derived Pleistocene age model: Uncertainty estimates, sedimentation variability, and nonlinear climate change, Paleoceanography, 19, https://doi.org/10.1029/2002PA000857, 2004.

Jevrejeva, S., Grinsted, A., and Moore, J. C.: Upper limit for sea level projections by 2100, Environmental Research Letters, 9, 104 008, https://doi.org/10.1088/1748-9326/9/10/104008, 2014.

Johnsen, S. J., Dahl-Jensen, D., Gundestrup, N., Steffensen, J. P., Clausen, H. B., Miller, H., Masson-Delmotte, V., Sveinbjörnsdottir, A. E., and White, J.: Oxygen isotope and palaeotemperature records from six Greenland ice-core stations: Camp Century, Dye-3, GRIP, GISP2, Renland and NorthGRIP, Journal of Quaternary Science, 16, 299–307, https://doi.org/10.1002/jqs.622, http://dx.doi.org/10.1002/jqs.622, 2001.

Kawamura, K., Severinghaus, J. P., Ishidoya, S., Sugawara, S., Hashida, G., Motoyama, H., Fujii, Y., Aoki, S., and Nakazawa, T.: Convective mixing of air in firn at four polar sites, Earth and Planetary Science Letters, 244, 672–682, http://dx.doi.org/10.1016/j.epsl.2006.02.017, 2006.

Kindler, P., Guillevic, M., Baumgartner, M., Schwander, J., Landais, A., and Leuenberger, M.: Temperature reconstruction from 10 to 120
5   kyr b2k from the NGRIP ice core, Climate of the Past, 10, 887–902, https://doi.org/10.5194/cp-10-887-2014, https://doi.org/10.5194/cp-10-887-2014, 2014.

Kingslake, J., Hindmarsh, R. C., Aðalgeirsdóttir, G., Conway, H., Corr, H. F., Gillet-Chaulet, F., Martín, C., King, E. C., Mulvaney, R., and Pritchard, H. D.: Full-depth englacial vertical ice sheet velocities measured using phase-sensitive radar, Journal of Geophysical Research: Earth Surface, 119, 2604–2618, https://doi.org/10.1002/2014JF003275, 2014.

10   Landais, A., Barnola, J. M., Kawamura, K., Caillon, N., Delmotte, M., Van Ommen, T., Dreyfus, G., Jouzel, J., Masson-Delmotte, V., Minster, B., Freitag, J., Leuenberger, M., Schwander, J., Huber, C., Etheridge, D., and Morgan, V.: Firn-air $\delta^{15}N$ in modern polar sites and glacial-interglacial ice: a model-data mismatch during glacial periods in Antarctica?, Quaternary Science Reviews, 25, 49–62, https://doi.org/10.1016/j.quascirev.2005.06.007, https://doi.org/10.1016/j.quascirev.2005.06.007, 2006.

Landais, A., Masson-Delmotte, V., Combourieu Nebout, N., Jouzel, J., Blunier, T., Leuenberger, M., Dahl-Jensen, D., and Johnsen, S.:
15   Millenial scale variations of the isotopic composition of atmospheric oxygen over Marine Isotopic Stage 4, Earth and Planetary Science Letters, 258, 101–113, https://doi.org/10.1016/j.epsl.2007.03.027, https://doi.org/10.1016/j.epsl.2007.03.027, 2007.

Landais, A., Dreyfus, G., Capron, E., Masson-Delmotte, V., Sanchez-Goñi, M. F., Desprat, S., Hoffmann, G., Jouzel, J., Leuenberger, M., and Johnsen, S.: What drives the millennial and orbital variations of $\delta^{18}O_{atm}$?, Quaternary Science Reviews, 29, 235–246, https://doi.org/10.1016/j.quascirev.2009.07.005, 2010.

20   Lundin, J. M., Stevens, C. M., Arthern, R., Buizert, C., Orsi, A., Ligtenberg, S. R., Simonsen, S. B., Cummings, E., Essery, R., Leahy, W., et al.: Firn Model Intercomparison Experiment (FirnMICE), Journal of Glaciology, 63, 401–422, https://doi.org/10.1017/jog.2016.114, 2017.

Martín, C., Hindmarsh, R. C., and Navarro, F. J.: Dating ice flow change near the flow divide at Roosevelt Island, Antarctica, by using a thermomechanical model to predict radar stratigraphy, Journal of Geophysical Research: Earth Surface (2003–2012), 111, 2006.

25   Martinerie, P., Lipenkov, V. Y., and Raynaud, D.: Correction of air-content measurements in polar ice for the effect of cut bubbles at the surface of the sample, Journal of Glaciology, 36, 299–303, https://doi.org/10.3189/002214390793701282, 1990.

Martinerie, P., Raynaud, D., Etheridge, D. M., Barnola, J. M., and Mazaudier, D.: Physical and climatic parameters which influence the air content in polar ice, Earth Planetary Science Letters, 112, 1–13, https://doi.org/10.1016/0012-821X(92)90002-D, 1992.

Masson-Delmotte, V., Hou, S., Ekaykin, A., Jouzel, J., Aristarain, A., Bernardo, R., Bromwich, D., Cattani, O., Delmotte, M., Falourd, S.,
30   et al.: A review of Antarctic surface snow isotopic composition: Observations, atmospheric circulation, and isotopic modeling, Journal of Climate, 21, 3359–3387, https://doi.org/10.1175/2007JCLI2139.1, 2008.

McKay, R., Golledge, N. R., Maas, S., Naish, T., Levy, R., Dunbar, G., and Kuhn, G.: Antarctic marine ice-sheet retreat in the Ross Sea during the early Holocene, Geology, 44, 7–10, https://doi.org/10.1130/G37315.1, 2016.

Mischler, J. A., Sowers, T. A., Alley, R. B., Battle, M., McConnell, J. R., Mitchell, L., Popp, T., Sofen, E., and Spencer,
35   M. K.: Carbon and hydrogen isotopic composition of methane over the last 1000 years, Global Biogeochemical Cycles, 23, https://doi.org/10.1029/2009gb003460, http://dx.doi.org/10.1029/2009GB003460, 2009.

Mitchell, L., Brook, E., Lee, J. E., Buizert, C., and Sowers, T.: Constraints on the Late Holocene Anthropogenic Contribution to the At-
mospheric Methane Budget, Science, 342, 964–966, https://doi.org/10.1126/science.1238920, https://doi.org/10.1126/science.1238920,
2013.

Mitchell, L. E., Brook, E. J., Sowers, T., McConnell, J. R., and Taylor, K.: Multidecadal variability of atmospheric methane, 1000-1800 C.E,
5   Journal of Geophysical Research, 116, G02 007, https://doi.org/10.1029/2010jg001441, http://dx.doi.org/10.1029/2010JG001441, 2011.

Mitchell, L. E., Buizert, C., Brook, E. J., Breton, D. J., Fegyveresi, J., Baggenstos, D., Orsi, A., Severinghaus, J., Alley, R. B., Albert, M.,
et al.: Observing and modeling the influence of layering on bubble trapping in polar firn, Journal of Geophysical Research: Atmospheres,
120, 2558–2574, https://doi.org/10.1002/2014JD022766, https://doi.org/10.1002/2014JD022766, 2015.

Nereson, N., Raymond, C., Waddington, E., and Jacobel, E.: Migration of the Siple Dome ice divide, West Antarctica, Journal of Glaciology,
10   44, 643–652, https://doi.org/10.3189/S0022143000002148, https://doi.org/10.3189/S0022143000002148, 1998.

NGRIP Community Members: High-resolution record of Northern Hemisphere climate extending into the last interglacial period, Nature,
431, 147–151, https://doi.org/10.1038/nature02805, ://000223746000034, 2004.

Nye, J.: Correction factor for accumulation measured by the thickness of the annual layers in an ice sheet, Journal of Glaciology, 4, 785–788,
https://doi.org/10.3189/S0022143000028367, 1963.

15   Parizek, B. R. and Alley, R. B.: Ice thickness and isostatic imbalances in the Ross Embayment, West Antarctica: model results, Global and
Planetary Change, 42, 265–278, https://doi.org/10.1016/j.gloplacha.2003.09.005, 2004.

Parrenin, F., Masson-Delmotte, V., Köhler, P., Raynaud, D., Paillard, D., Schwander, J., Barbante, C., Landais, A., Wegner, A., and Jouzel,
J.: Synchronous change of atmospheric CO$_2$ and Antarctic temperature during the last deglacial warming, Science, 339, 1060–1063,
https://doi.org/10.1126/science.1226368, https://doi.org/10.1126/science.1226368, 2013.

20   Petit, J. R., Jouzel, J., Raynaud, D., Barkov, N. I., Barnola, J. M., Basile, I., Bender, M., Chappellaz, J., Davis, M., Delaygue, G., Delmotte, M.,
Kotlyakov, V. M., Legrand, M., Lipenkov, V. Y., Lorius, C., Pepin, L., Ritz, C., Saltzman, E., and Stievenard, M.: Climate and atmospheric
history of the past 420,000 years from the Vostok ice core, Antarctica, Nature, 399, 429–436, https://doi.org/10.1038/20859, 1999.

Petrenko, V. V., Severinghaus, J. P., Brook, E. J., Reeh, N., and Schaefer, H.: Gas records from the West Greenland ice margin covering the
Last Glacial Termination: a horizontal ice core, Quaternary Science Reviews, 25, 865–875, https://doi.org/10.1016/j.quascirev.2005.09.
25   005, 2006.

Pollard, D., DeConto, R. M., and Alley, R. B.: Potential Antarctic Ice Sheet retreat driven by hydrofracturing and ice cliff failure, Earth and
Planetary Science Letters, 412, 112–121, https://doi.org/10.1016/j.epsl.2014.12.035, 2015.

Price, S., Conway, H., and Waddington, E.: Evidence for late Pleistocene thinning of Siple Dome, West Antarctica, Journal of Geophysical
Research: Earth Surface, 112, https://doi.org/10.1029/2006JF000725, https://doi.org/10.1029/2006JF000725, 2007.

30   Pyne, R. L., Keller, E. D., Canessa, S., Bertler, N. A., Pyne, A. R., Mandeno, D., Vallelonga, P., Semper, S., Kjær, H. A., Hutchinson, E., and
Baisden, W. T.: A novel approach to process brittle ice for continuous flow analysis of stable water isotopes, Journal of Glaciology, 64,
289–299, https://doi.org/10.1017/jog.2018.19, 2018.

Raynaud, D. and Whillans, I.: Air content of the Byrd core and past changes in the West Antarctic ice sheet, Annals of Glaciology, 3,
269–273, https://doi.org/10.3189/S0260305500002901, 1982.

35   Raynaud, D., Lipenkov, V., Lemieux-Dudon, B., Duval, P., Loutre, M. F., and Lhomme, N.: The local insolation signature of air con-
tent in Antarctic ice. A new step toward an absolute dating of ice records, Earth and Planetary Science Letters, 261, 337–349,
https://doi.org/10.1016/j.epsl.2007.06.025, https://doi.org/10.1016/j.epsl.2007.06.025, 2007.

Rhodes, R. H., Faïn, X., Stowasser, C., Blunier, T., Chappellaz, J., McConnell, J. R., Romanini, D., Mitchell, L. E., and Brook, E. J.: Continuous methane measurements from a late Holocene Greenland ice core: Atmospheric and in-situ signals, Earth and Planetary Science Letters, 368, 9–19, https://doi.org/10.1016/j.epsl.2013.02.034, https://doi.org/10.1016/j.epsl.2013.02.034, 2013.

Rhodes, R. H., Brook, E. J., Chiang, J. C., Blunier, T., Maselli, O. J., McConnell, J. R., Romanini, D., and Severinghaus, J. P.: Enhanced tropical methane production in response to iceberg discharge in the North Atlantic, Science, 348, 1016–1019, https://doi.org/10.1126/science.1262005, https://doi.org/10.1126/science.1262005, 2015.

Rhodes, R. H., Brook, E. J., McConnell, J. R., Blunier, T., Sime, L. C., Faïn, X., and Mulvaney, R.: Atmospheric methane variability: Centennial-scale signals in the Last Glacial Period, Global Biogeochemical Cycles, 31, 575–590, https://doi.org/10.1002/2016GB005570, https://doi.org/10.1002/2016GB005570, 2017.

Robin, G. d. Q. and Adie, R. J.: The ice cover, in: Antarctic research: a review of British scientific achievement in Antarctica, edited by Priestley, R. E., Adie, R. J., and Robin, G. d. Q., pp. 100–117, Butterworth & Co Publishers Ltd, London, 1964.

Sapart, C. J., Monteil, G., Prokopiou, M., van de Wal, R. S. W., Kaplan, J. O., Sperlich, P., Krumhardt, K. M., van der Veen, C., Houweling, S., Krol, M. C., Blunier, T., Sowers, T., Martinerie, P., Witrant, E., Dahl-Jensen, D., and Röckmann, T.: Natural and anthropogenic variations in methane sources during the past two millennia, Nature, 490, 85–88, http://dx.doi.org/10.1038/nature11461, 2012.

Schoof, C.: Ice sheet grounding line dynamics: Steady states, stability, and hysteresis, Journal of Geophysical Research: Earth Surface, 112, https://doi.org/10.1029/2006JF000664, 2007.

Schwander, J.: The transformation of snow to ice and the occlusion of gases, in: The Environmental Record in Glaciers and Ice Sheets, edited by Oescher, H. and Langway, C., pp. 53–67, John Wiley, New York, 1989.

Schwander, J., Sowers, T., Barnola, J. M., Blunier, T., Fuchs, A., and Malaize, B.: Age scale of the air in the summit ice: Implication for glacial-interglacial temperature change, Journal of Geophysical Research: Atmospheres, 102, 19 483–19 493, https://doi.org/10.1029/97JD01309, 1997.

Scott, R. F.: The Voyage of the Discovery, vol. 1, Smith, Elder, 1907.

Severinghaus, J. P., Beaudette, R., Headly, M. A., Taylor, K., and Brook, E. J.: Oxygen-18 of O_2 Records the Impact of Abrupt Climate Change on the Terrestrial Biosphere, Science, 324, 1431–1434, https://doi.org/10.1126/science.1169473, https://doi.org/10.1126/science.1169473, 2009.

Shepherd, A., Wingham, D., and Rignot, E.: Warm ocean is eroding West Antarctic ice sheet, Geophysical Research Letters, 31, https://doi.org/10.1029/2004GL021106, 2004.

Shipp, S., Anderson, J., and Domack, E.: Late Pleistocene-Holocene retreat of the West Antarctic Ice Sheet system in the Ross Sea: part 1—geophysical results, Geological Society of America Bulletin, 111, 1486–1516, https://pubs.geoscienceworld.org/gsa/gsabulletin/article-abstract/111/10/1486/183430/late-pleistocene-holocene-retreat-of-the-west?redirectedFrom=fulltext, 1999.

Sigl, M., Fudge, T. J., Winstrup, M., Cole-Dai, J., Ferris, D., McConnell, J. R., Taylor, K. C., Welten, K. C., Woodruff, T. E., Adolphi, F., Bisiaux, M., Brook, E. J., Buizert, C., Caffee, M. W., Dunbar, N. W., Edwards, R., Geng, L., Iverson, N., Koffman, B., Layman, L., Maselli, O. J., McGwire, K., Muscheler, R., Nishiizumi, K., Pasteris, D. R., Rhodes, R. H., and Sowers, T. A.: The WAIS Divide deep ice core WD2014 chronology - Part 2: Annual-layer counting (0-31 ka BP), Climate of the Past, 12, 769–786, https://doi.org/10.5194/cp-12-769-2016, https://doi.org/10.5194/cp-12-769-2016, 2016.

Sowers, T., Bender, M., and Raynaud, D.: Elemental and isotopic composition of occluded O_2 and N_2 in polar ice, Journal of Geophysical Research: Atmospheres, 94, 5137–5150, https://doi.org/10.1029/JD094iD04p05137, http://dx.doi.org/10.1029/JD094iD04p05137, 1989.

Sowers, T., Bender, M., Labeyrie, L., Martinson, D., Jouzel, J., Raynaud, D., Pichon, J. J., and Korotkevich, Y. S.: A 135,000-year Vostok-Specmap Common temporal framework, Paleoceanography, 8, 737–766, https://doi.org/10.1029/93PA02328, 1993.

Steig, E. J., Fastook, J. L., Zweck, C., Goodwin, I. D., Licht, K. J., White, J. W., and Ackert, R. P.: West Antarctic ice sheet elevation changes, in: The West Antarctic Ice Sheet: Behavior and Environment, edited by Alley, R. B. and Bindschadle, R. A., Antarctic Research Series, pp. 75–90, Wiley Online Library, https://doi.org/10.1029/AR077p0075, 2001.

Stenni, B., Curran, M. A., Abram, N. J., Orsi, A., Goursaud, S., Masson-Delmotte, V., Neukom, R., Goosse, H., Divine, D., Van Ommen, T., et al.: Antarctic climate variability on regional and continental scales over the last 2000 years, Climate of the Past, 13, 1609, https://doi.org/10.5194/cp-13-1609-2017, 2017.

Stone, J. O., Balco, G. A., Sugden, D. E., Caffee, M. W., Sass, L. C., Cowdery, S. G., and Siddoway, C.: Holocene deglaciation of Marie Byrd land, West Antarctica, Science, 299, 99–102, https://doi.org/10.1126/science.1077998, 2003.

Stowasser, C., Buizert, C., Gkinis, V., Chappellaz, J., Schüpbach, S., Bigler, M., Faïn, X., Sperlich, P., Baumgartner, M., Schilt, A., and Blunier, T.: Continuous measurements of methane mixing ratios from ice cores, Atmospheric Measurement Techniques, 5, 999–1013, https://doi.org/10.5194/amt-5-999-2012, http://dx.doi.org/10.5194/amt-5-999-2012, 2012.

Stuiver, M., Denton, G. H., Hughes, T. J., and Fastook, J. L.: History of the marine ice sheet in West Antarctica during the last glaciation: a working hypothesis, in: The Last Great Ice Sheets, edited by Denton, G. H. and Hughes, T. J., pp. 319–436, John Wiley & Sons, New York, 1981.

Svensson, A., Andersen, K. K., Bigler, M., Clausen, H. B., Dahl-Jensen, D., Davies, S., Johnsen, S. J., Muscheler, R., Parrenin, F., Rasmussen, S. O., et al.: A 60,000 year Greenland stratigraphic ice core chronology, Climate of the Past, 4, 47–57, https://doi.org/10.5194/cp-4-47-2008, https://doi.org/10.5194/cp-4-47-2008, 2008.

Thorsteinsson, T. and Waddington, E. D.: Folding in strongly anisotropic layers near ice-sheet centers, Annals of Glaciology, 35, 480–486, https://doi.org/10.3189/172756402781816708, 2002.

Tuohy, A., Bertler, N., Neff, P., Edwards, R., Emanuelsson, D., Beers, T., and Mayewski, P.: Transport and deposition of heavy metals in the Ross Sea Region, Antarctica, Journal of Geophysical Research: Atmospheres, 120, http://dx.doi.org/10.1002/2015JD023293, 2015.

Waddington, E., Conway, H., Steig, E., Alley, R., Brook, E., Taylor, K., and White, J.: Decoding the dipstick: Thickness of Siple Dome, West Antarctica, at the last glacial maximum, Geology, 33, 281–284, https://doi.org/10.1130/G21165.1, 2005.

Waddington, E. D., Bolzan, J. F., and Alley, R. B.: Potential for stratigraphic folding near ice-sheet centers, Journal of Glaciology, 47, 639–648, https://doi.org/10.3189/172756501781831756, 2001.

WAIS Divide Project Members: Onset of deglacial warming in West Antarctica driven by local orbital forcing, Nature, 500, 440–444, https://doi.org/10.1038/nature12376, http://dx.doi.org/10.1038/nature12376, 2013.

Weertman, J.: Stability of the junction of an ice sheet and an ice shelf, Journal of Glaciology, 13, 3–11, https://doi.org/10.3189/S0022143000023327, 1974.

Whitehouse, P. L., Bentley, M. J., and Le Brocq, A. M.: A deglacial model for Antarctica: geological constraints and glaciological modelling as a basis for a new model of Antarctic glacial isostatic adjustment, Quaternary Science Reviews, 32, 1–24, https://doi.org/10.1016/j.quascirev.2011.11.016, 2012.

Winstrup, M.: A Hidden Markov Model Approach to Infer Timescales for High-Resolution Climate Archives, in: AAAI, pp. 4053–4061, 2016.

Winstrup, M., Svensson, A. M., Rasmussen, S. O., Winther, O., Steig, E. J., and Axelrod, A. E.: An automated approach for annual layer counting in ice cores, Climate of the Past, 8, 1881–1895, https://doi.org/10.5194/cp-8-1881-2012, https://doi.org/10.5194/cp-8-1881-2012, 2012.

Winstrup, M., Vallelonga, P., Kjær, H. A., Fudge, T. J., Lee, J. E., Riis, M. H., Edwards, R., Bertler, N. A. N., Blunier, T., Brook, E. J.,
5   Buizert, C., Ciobanu, G., Conway, H., Dahl-Jensen, D., Ellis, A., Emanuelsson, B. D., Keller, E. D., Kurbatov, A., Mayewski, P., Neff, P. D., Pyne, R., Simonsen, M. F., Svensson, A., Tuohy, A., and Wheatley, S.: A 2700-year annual timescale and accumulation history for an ice core from Roosevelt Island, West Antarctica, Climate of the Past Discussions, 2017, 1–46, https://doi.org/10.5194/cp-2017-101, https://doi.org/10.5194/cp-2017-101, 2017.

Wolff, E. W., Chappellaz, J., Blunier, T., Rasmussen, S. O., and Svensson, A.: Millennial-scale variability during the last glacial: The ice
10   core record, Quaternary Science Reviews, 29, 2828–2838, https://doi.org/10.1038/ngeo442, 2010.

Climate
of the Past

Open Access

EGU

Discussions
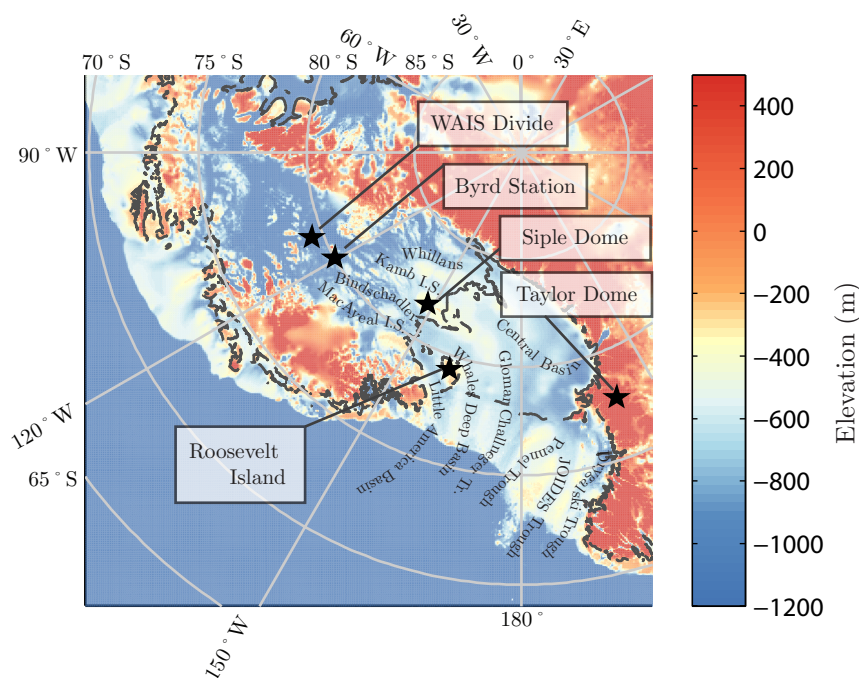
Figures

Figure 1. Map of bedrock elevation in the Ross Sea Sector of Antarctica (referenced to WGS84 datum) (Fretwell et al., 2013). Gray dashed lines indicate ice sheet grounding lines and ice margins. Locations of the RICE (Roosevelt Island), Siple Dome, Byrd Station, WAIS Divide, and Taylor Dome ice cores are marked with black stars.

Climate
of the Past
Discussions
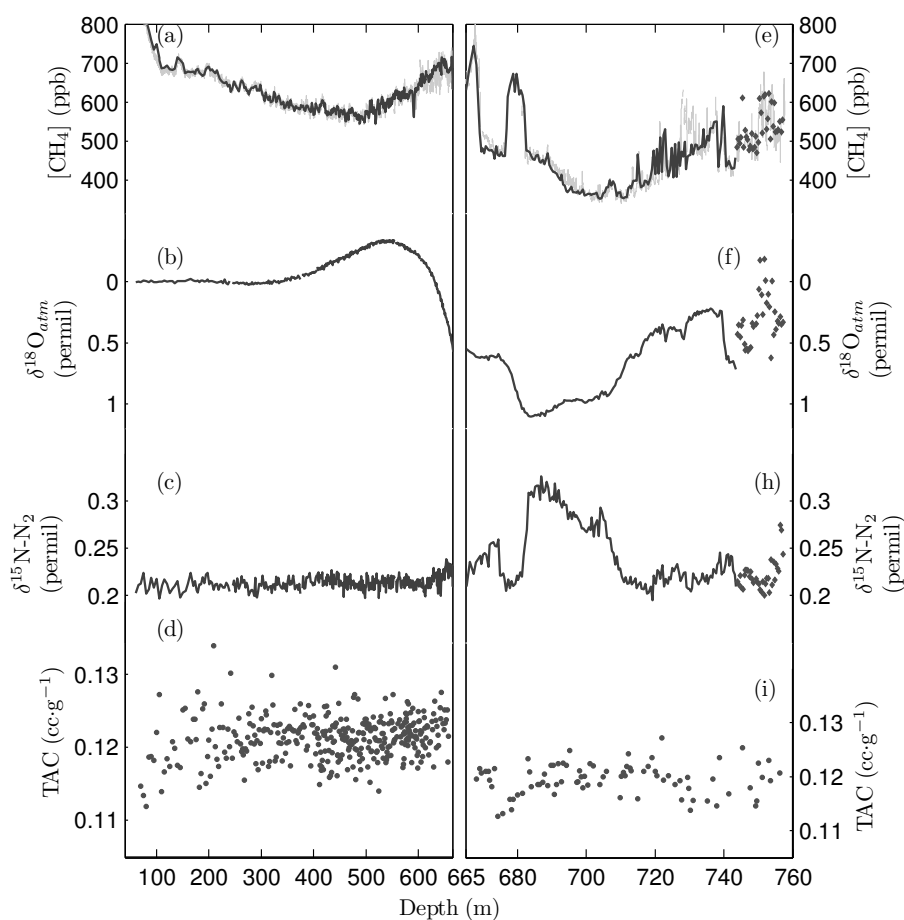
Figure 2. Gas data from the RICE ice core. Left panel (a-e) (60-665 m) covers the last 11.26 ka; Right panel (f-j) (665-760 m) covers measurements from 11.26-83 ka and measurements from the 7 m of ice below the dated section. (a, f) Continuous methane measurements, gray, between 0-726 m depth are calibrated to discrete methane measurements, black. Beyond 726 m depth, raw CFA methane measurements are plotted. (b, g) $\delta^{18}O_{atm}$ measurements are corrected for gravitational enrichment in the firn layer using δ^{15}N-N_2 (c, h) . (d, i) TAC was measured in conjunction with discrete methane.
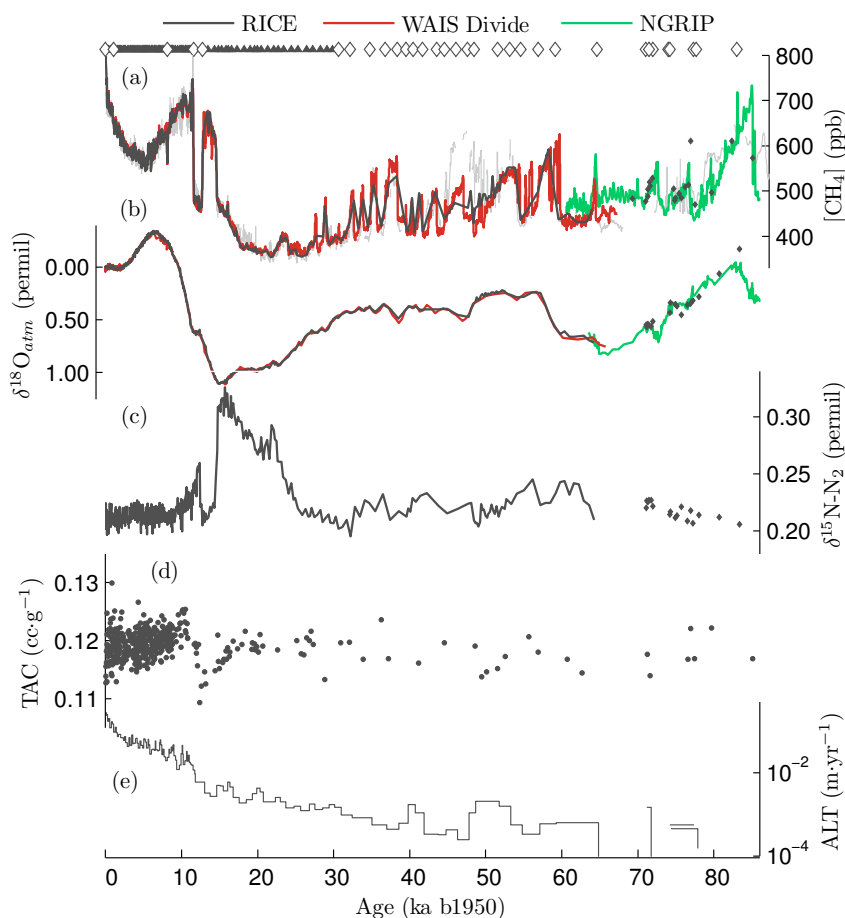
Figure 3. Gas data from the RICE ice core plotted on the RICE17 age scale. (a) RICE methane and (b) $\delta^{18}O_{atm}$ records (gray) shown in comparison to reference records from the WAIS Divide ice core on the WD2014 age scale (Buizert et al., 2015) (red) and NGRIP ice core (Baumgartner et al., 2014; Landais et al., 2007) on a modified GICC05modelext chronology (Wolff et al., 2010) (green). Solid triangles above panel (a) are gas age constraints from a Monte Carlo analysis, open diamonds are prior ACPs from visual matching. The (c) RICE δ^{15}N-N$_2$ partially constrains a firn densification model used to estimate the ice age-gas age offset. (d) RICE TAC measurements. (e) Mean annual layer thickness calculated from gas age control points adjusted for Δage.
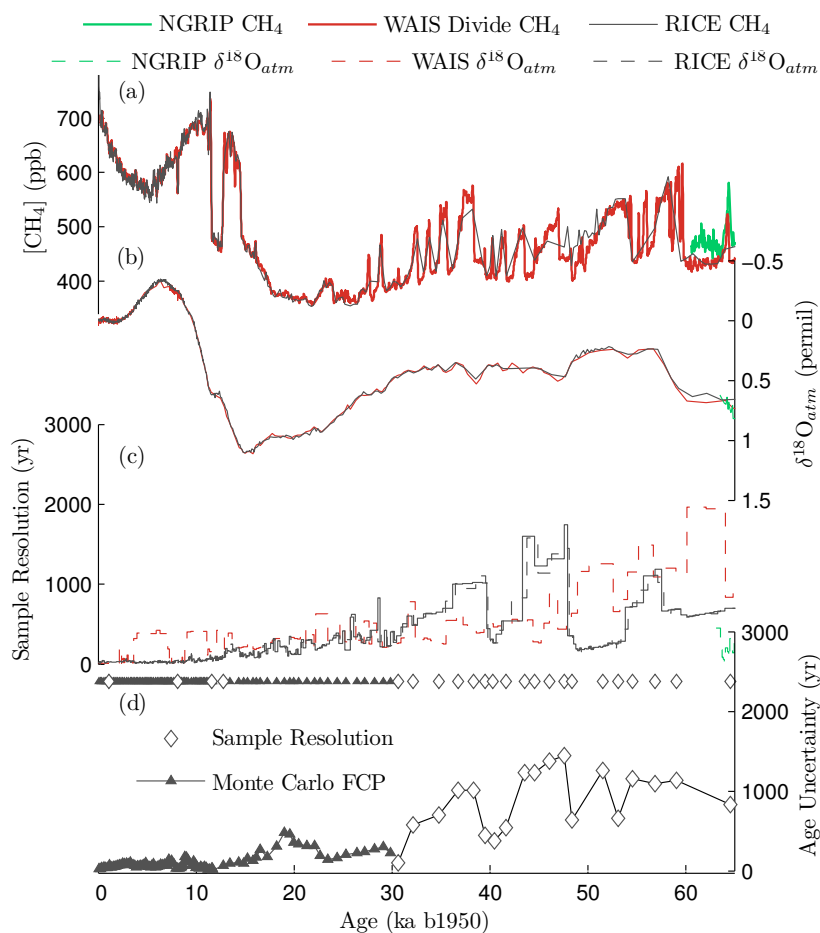
Figure 4. RICE ice core age uncertainty. (a) Methane and (b) $\delta^{18}O_{atm}$ records from the RICE (gray), WAIS Divide (Rhodes et al., 2015) (red), and NGRIP ice cores (Baumgartner et al., 2014) (green). (c) Sample resolution for methane (solid lines) and $\delta^{18}O_{atm}$ (dashed lines) for the various cores. (d) Gas age uncertainty, relative to WD2014, for ages determined from a Monte Carlo analysis (solid triangles) and for extended gas age control points (open diamonds).
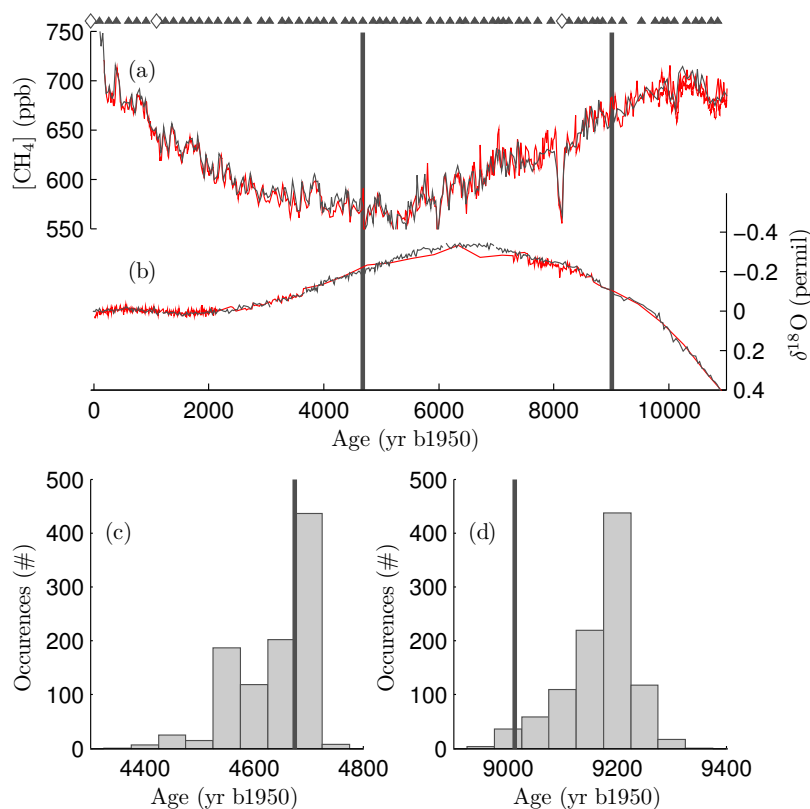
Figure 5. (a) RICE methane and (b) $\delta^{18}O_{atm}$ records matched to those from the WAIS Divide ice core (Rhodes et al., 2015; Buizert et al., 2015) (red lines) between present and 11.7 ka. FCPs from Monte Carlo routine are shown as solid triangles, prior constraints are shown as open diamonds. Lower panels (c, d) show the distribution of the gas ages for two particular depths, 459.05 m (4675 yr BP) (c) and 621.28 m (9012 yr BP) (d), resulting from the Monte Carlo analysis. The final age of these depths, resulting from the best realization, are shown as vertical gray lines.

Climate
of the Past

Open Access

Discussions

EGU
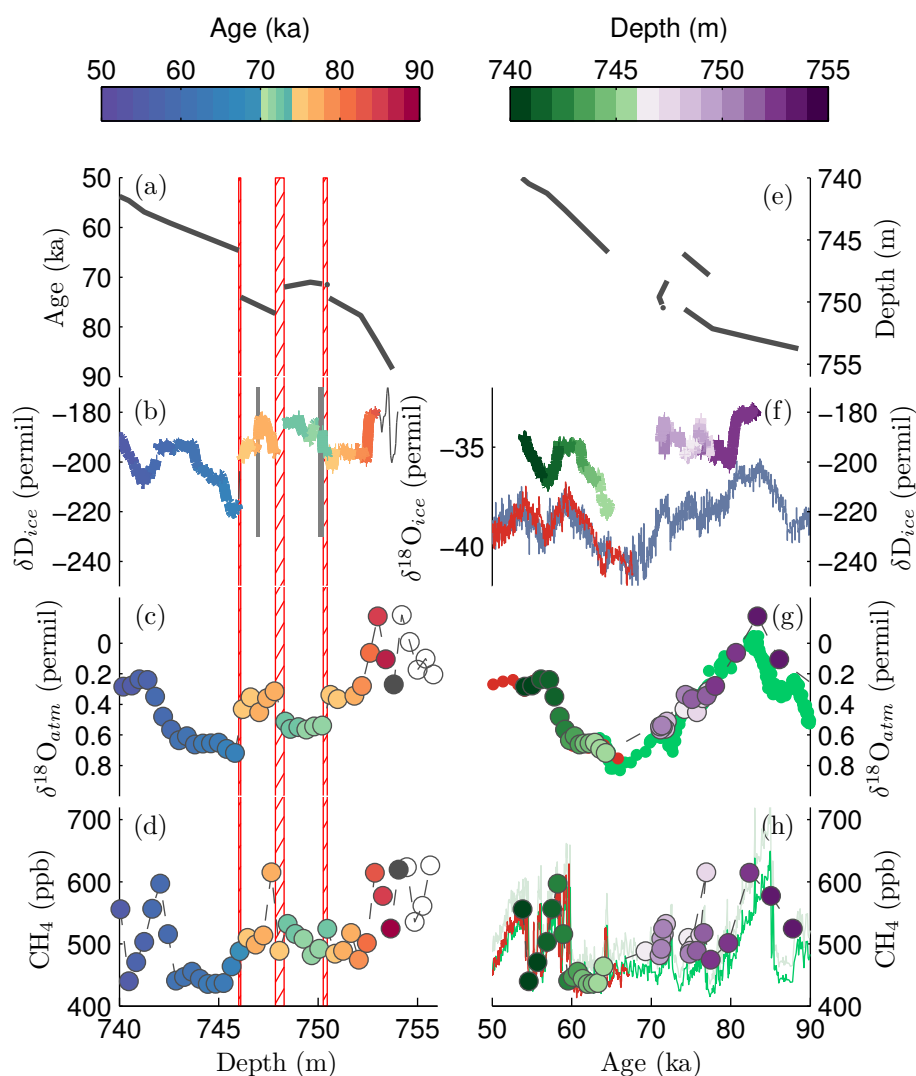
Figure 6. (a) Depth-age relationship and evidence of an age reversal within the RICE ice core from (b) δD, (c) $\delta^{18}O_{atm}$, and (d) methane data. (b-d) Measurements are plotted against depth and color coded according to the age of the sample. (a-d) Red hatched bars represent discontinuities, where periods of climate history appear to be missing. Solid gray bars in (b) are measurement gaps in the δD record associated with large changes in δD. Repetitions of clusters of data with similar methane and $\delta^{18}O_{atm}$ values best dated to DO-20 are observed both above and below a cluster of depths best dated to DO-19. (e-h) The depth-age relationship and measurements are plotted against the age of the sample and color coded according to depth. WAIS Divide data (red), NGRIP (green), and the EDML $\delta^{18}O_{ice}$ record (blue).

Climate
of the Past

Discussions

Open Access

EGU
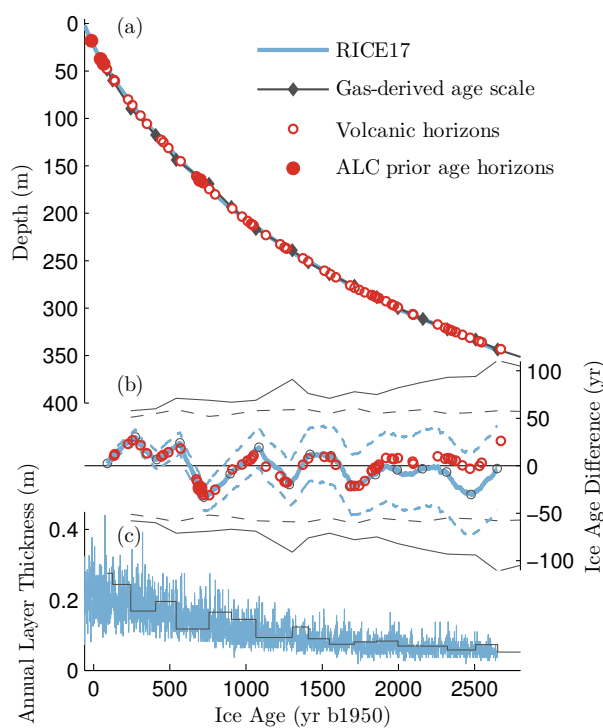
Figure 7. Comparison of the gas-derived (gray) and the annual layer counted ice age scale (blue, Winstrup et al. 2017). Six absolute age markers (closed red circles) were identified and an additional 67 volcanic horizons were cross correlated to volcanic horizons in the WAIS Divide core (plotted on WD2014 ice age scale, open red circles, Winstrup et al. 2017). (b) Difference in ice age between the gas-derived ice age scale and annual layer counts; positive values indicate that at the same depth the annual layer counts is older than in the gas-derived age scale. Uncertainty estimates of the gas-derived ice age scale (solid gray lines), of the Δage estimate only (dashed gray lines), and of the annual layer counted age scale (blue dashed lines). (c) Interpretations of annual layer thickness from the gas-derived ice age scale and annual layer interpretations.

Climate
of the Past
Discussions
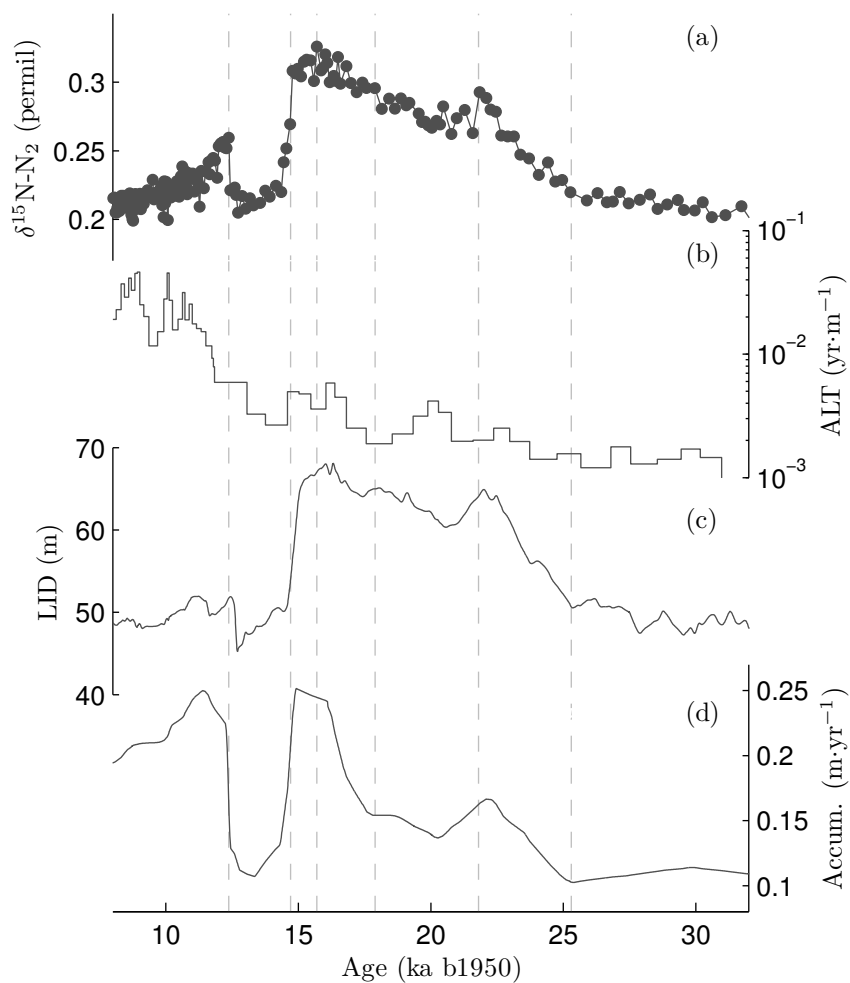
Figure 8. Comparison of (a) δ^{15}N-N$_2$, (b) annual layer thickness implied from depth-age scale, (c) lock-in depth (LID), and (d) accumulation reconstructions from the RICE ice core. Lock-in depth and accumulation is calculated with a dynamic Herron-Langway firn densification model.

Tables

Climate
of the Past
Discussions

Open Access

EGU

Table 1. Prior gas age constraints and uncertainty are based on matching of features in the atmospheric history of methane and $\delta^{18}O_{atm}$. Name or description of feature are given in the notes and the primary parameter used to identify the feature is provided as the identifying variable. Age uncertainty is related to the duration of the feature.

Depth (m)	Gas_Age (yr)	σ (yr)	Identifying Variable	Notes
48.57	-55.4	7	Modern LID	
239.000	1092	45	CH$_4$	
591.000	8140	30	CH$_4$	8.2 ka event
669.150	11580	30	CH$_4$	Younger-Dryas — Preboreal
677.300	12780	57	CH$_4$	Bølling-Allerød — Younger Dryas
719.300	30660	100	CH$_4$	GI 5.1 Termination
720.700	32150		CH$_4$	GI 5.2 Termination
722.800	34780		CH$_4$	GI 7 Termination
723.900	36750		CH$_4$	GI 8 Termination
724.600	38370		CH$_4$	GI 8 Onset
725.310	39530		CH$_4$	Mid-GS 9 Methane Event
726.850	40332		CH$_4$	GI 9 Onset
728.090	41643		CH$_4$	GI 10 Onset
728.720	43544		CH$_4$	GI 11 Onset
729.050	44562		CH$_4$	GI 12 Termination
729.680	46100		$\delta^{18}O_{atm}$	
730.050	47620		$\delta^{18}O_{atm}$	GI 12 Onset
730.950	48420		$\delta^{18}O_{atm}$	Mid-GS 12 Methane Event
737.260	51570		$\delta^{18}O_{atm}$	
739.650	53115		$\delta^{18}O_{atm}$	
740.470	54595		$\delta^{18}O_{atm}$	GI 14 Onset
741.250	56885		$\delta^{18}O_{atm}$	(MIS 4/3 Transition)
742.550	59100		$\delta^{18}O_{atm}$	GI 17.1a Onset (MIS 4/3 Transition)
746.000	64600		δD, $\delta^{18}O_{atm}$, CH$_4$	Top Depth of discontinuity
746.100	74000		δD, $\delta^{18}O_{atm}$, CH$_4$	Bottom Depth of discontinuity
747.850	77300		δD, $\delta^{18}O_{atm}$, CH$_4$	Depth of reversal in δD
748.290	72000		$\delta^{18}O_{atm}$	First $\delta^{18}O_{atm}$ sample clearly in DO-19 grouping
749.600	71000		$\delta^{18}O_{atm}$, CH$_4$	Depth of youngest part of reversal in δD
750.460	71500		CH$_4$	Deepest sample clearly related to reversal grouping
750.560	74200		$\delta^{18}O_{atm}$, CH$_4$	Shallowest sample related to return to DO20 values
752.150	77700		$\delta^{18}O_{atm}$, CH$_4$	Last $\delta^{18}O_{atm}$ sample clearly part of DO20
752.950	83000		$\delta^{18}O_{atm}$	Minima in $\delta^{18}O_{atm}$, matching values observed in NGRIP and EDML for MIS 5a
753.750	88500		$\delta^{18}O_{atm}$	Enriched $\delta^{18}O_{atm}$, MIS 5b?

Table 2. Model Parameters used for optimized correlation routine. Code for routine can be found in supplementary material.

Variable	Description	0-670 m	670-718.13 m
Model Parameters:			
Runs	# of realizations in Monte Carlo Analysis	1000	1000
N	# of subsections	76	25
Δt	Duration of subsections	154 yrs	726 yrs
k	# of refinements to perturbation	13	13
n_{rep}	# of repetitions before moving to next refinement	20	20
Perturbation Conditions:			
$\overline{A}_{max}$	Maximum "Accumulation"	75 cm·yr^{-1}	75 cm·yr^{-1}
$\overline{A}_{min}$	Minimum "Accumulation"	0 cm·yr^{-1}	0 cm·yr^{-1}
$\Delta t/\Delta t_{prior}$	Relative change in duration of subsection from prior	10x	10x
$\overline{A}_i/\overline{A}_{i-1}$	Maximum relative change of "accumulation rate" between subsequent subsections	2x	2x

Appendix Tables

Table A1. Model Parameters used for steady-state Herron-Langway model.

Description	Mean	σ	Distribution
δ^{15}N-N$_2$		0.0027‰	normal
Modern temperature	-23.5°C	3°C	normal
Isotope sensitivity	6 ‰·K^{-1}	1.2 ‰·K^{-1}	normal
Surface firn density	400 kg·m^{-3}	.05 kg·m^{-3}	normal
Convective zone thickness	2 m	2 m	uniform
Geothermal induced temperature gradient	-0.6 K	0.6 K	uniform

Climate
of the Past
Discussions

Open Access

Table A2. Calibration of the RICE CFA methane dataset is performed by comparison to the RICE discrete methane dataset with corrections for instrument sensitivity and instrument drift. Calibration is done for different segments of the core. Quality of the fit is described by the R^2 statistic comparing calibrated values of the sub-sampled CFA methane record to discrete measurements.

Depth Range	Instr.	Drift	R^2
0-500 m	$C_{final} = C_{raw} \cdot 1.1079 + 25.0900$		0.9854
500-680 m	$C_{final} = C_{raw} \cdot 0.9440 + 10.9337$	$+ \quad t_{meas} \cdot 4.0181 \cdot 10^{-5} - 1.4013 \cdot 10^{-5}$	0.9239
682-726 m	$C_{final} = C_{raw} \cdot 0.8869 + 29.2036$		